Contents of the File

1. Reply to the comments from Reviewer-1

We are thankful to the reviewer for acknowledging the importance of our work and highlighting the point that spatially and temporally varying compensation depths in the surface restoration models are indeed important. The reviewer also gave important comments to further improve the manuscript. As per his/her comments, analysis has been carried out and the manuscript is revised as below.

A point-by-point reply to reviewer's comment is as follows. For clarity the comments are shown in blue fonts.

1. The introduction is too long with too many unnecessary narrations. I generally have a feeling after reading introduction several times, the paragraphs are not carrying a 'specific message per paragraphs'. Introductions required to be synchronized.

We thank the reviewer for a thorough reading and understanding of the manuscript. We agree to some extend to the reviewer's opinion that the introduction could be trimmed a bit for more clarity and avoid too long unnecessary narrations. This has been resolved in the revised manuscript.

2. The biogeochemical model used in the study requires a little more details.

We kindly request the reviewer to go through the appendix –A of the manuscript where we have given the entire details of the model. We feel that it is better to leave the details in the Appendix to avoid distraction from the main message and to keep the main manuscript more focused. Thank you.

3. Author(s) may explore the possibility of quantifying both the biological and solubility pumps which play an important role in the Indian Ocean upwelling zones.

This was a very valuable suggestion, to further highlight our claim that the biological pump is better represented by the new parameterization. Though this was already stated in the earlier version of the manuscript an explicit quantification and narration was missing. In the revised form we have resolved this issue.

As per the reviewer's suggestions we have conducted two additional simulations to quantify the impact of varying compensation depth in the biological and solubility pumps over the upwelling zones. The simulations were carried out from 1961 to 2010, however for further analysis; the data from 1990 to 2010 is utilized as done in the previous version of this manuscript. In these new simulations more model diagnostics were saved such as explicit profiles of biological pump in terms of DIC and calcite. We have adopted the methodology of Louanchi et. al., (1996) for the computation of the tendency of dissolved inorganic carbon (DIC) caused by the biological and solubility pumps.

The biological effect on DIC is calculated from the biomass production and calcite formation in the production zone expressed as below:

$$\left(\frac{\partial DIC}{\partial t}\right)_b = \left(\frac{\partial PO_4}{\partial t}\right)_b * R_{C:P} - J_{Ca} \qquad (1)$$

The total tendency due to DIC in the mixed layer depth is the sum of both the pumps (Louanchi et al., 1996).

$$\left(\frac{\partial DIC}{\partial t}\right)_{total} = \left(\frac{\partial DIC}{\partial t}\right)_b + \int_x \int_y \Phi dx\, dy \qquad (2)$$

Where $\left(\frac{\partial DIC}{\partial t}\right)_b$ is the evolution of DIC due to the impact of biology. $\left(\frac{\partial PO_4}{\partial t}\right)_b$ is the rate of change of phosphate which represents the biological production in the model multiplied by the Redfield ratio ($R_{C:P}$ = 117:1) calculated in terms of carbon and J_{Ca} represents the calcite formation in the model. The solubility pump is calculated by integrating the surface fluxes. Results are discussed as below.

Effect of varZc parameterization in strengthening the pump intensity over the selected upwelling regions are shown in Figure 1 (a-d) of this response note. The spatially and temporally varying compensation depth (varZc) strengthened the biological pump and solubility pump in the model as compared to constant Zc simulations.

Figure 1a shows the comparison of both solubility and biological pump over the western Arabian Sea (WAS). The analysis proves that draw down of dissolved inorganic carbon(DIC) from the production zone due to biological effect is increased by the varZc thereby strengthening the biological pump in the model.

The annual mean DIC variation due to biological effect in constZc simulation is 45.49 ± 14.3 g C m^{-2} yr^{-1}. However varZc parameterization increases the DIC variation due to biological pump to 126.6 ± 24.3 g C m^{-2} yr^{-1}. This is clear that the varZc has increased the strength of biological pump as evidenced by the increase in DIC variations of the production zone due to biological effects.

The table 1 summarizes the results of the impact of the biological pump over DIC in the model under constZc and varZc simulations.

Biological Pump ($gC\ m^{-2}\ yr^{-1}$)	**constZc**		**varZc**	
	JJAS Mean	**Annual Mean**	**JJAS Mean**	**Annual Mean**
WAS	45.18 ± 14.8	45.49 ± 14.38	151.7 ± 23.8	126.67 ± 24.3
SLD	89.39 ± 58.1	108.65 ± 48.6	156.07 ± 48.4	161.15 ± 43.5
SC	235.54 ± 95.4	155.21 ± 67.4	319.16 ± 94.9	222.92 ± 68.7
SCTR	30.49 ± 13.4	26.81 ± 16.8	103.13 ± 19.6	83.98 ± 23.6

Table 2 summarizes the impact of varZc over the solubility pump in the model

Solubility Pump ($gC\ m^{-2}\ yr^{-1}$)	**constZc**		**varZc**	
	JJAS Mean	**Annual Mean**	**JJAS Mean**	**Annual Mean**
WAS	17.29 ± 3.5	9.63 ± 2.1	27.72 ± 4.8	12.92 ± 2.7
SLD	-0.09 ± 2.4	-0.32 ± 2.3	2.9 ± 3.5	1.31 ± 3.5
SC	7.22 ± 6.9	2.56 ± 3.8	18.17 ± 12.1	6.43 ± 6.0
SCTR	-3.95 ± 3.7	-0.35 ± 2.3	-0.61 ± 5.3	-0.86 ± 2.8

The above analysis clearly shows that the spatially and temporally varying compensation depth significantly affects both solubility and biological pumps in the upwelling zones.

In addition, the results are consistent with the export production profile which is indirectly a measure of the biological pump in the model. These additional findings are now added to the revised manuscript.

Reference

Louanchi. F., N. Metzl., and Alain Poisson: Modelling the monthly sea surface f_{CO2} fields in the Indian Ocean, Marine Chemistry, 55, 265 – 279, 1996.

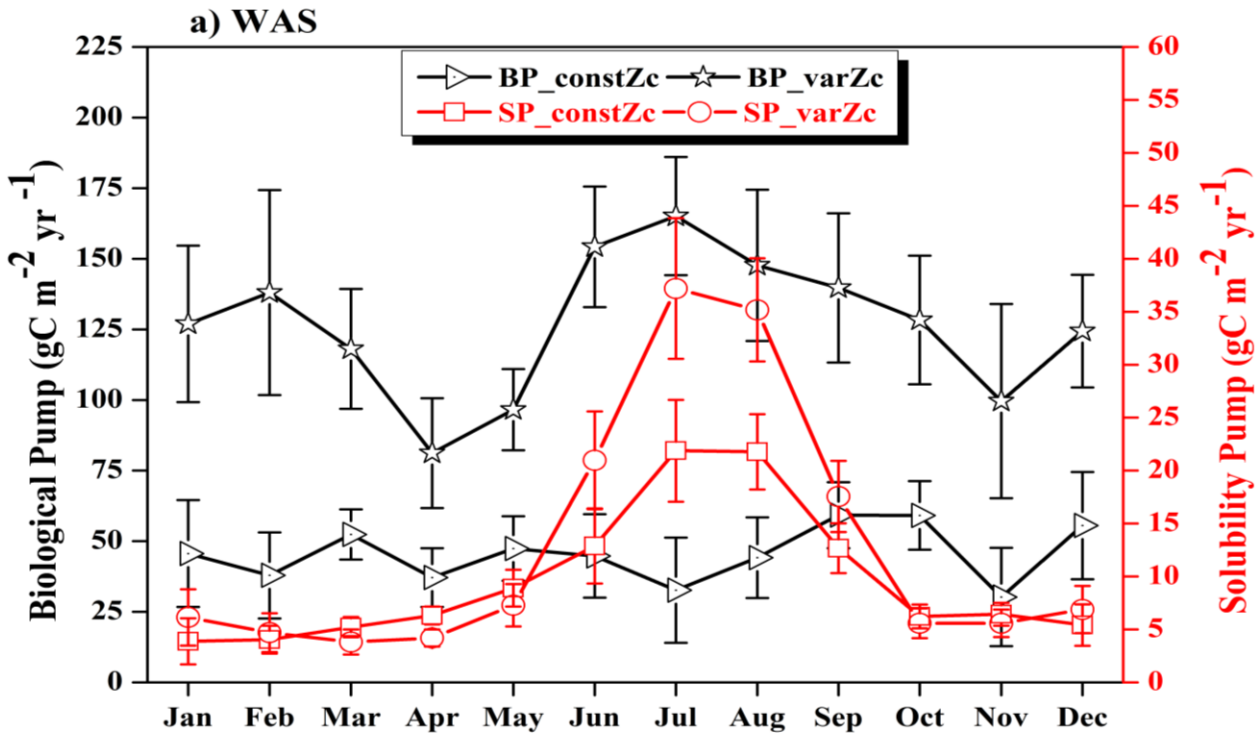
a) WAS
BP_constZc
BP_varZc
SP_constZc
SP_varZc
Biological Pump (gC m-2 yr-1)
Solubility Pump (gC m-2 yr-1)
0
25
50
75
100
125
150
175
200
225
0
5
10
15
20
25
30
35
40
45
50
55
60
Jan
Feb
Mar
Apr
May
Jun
Jul
Aug
Sep
Oct
Nov
Dec

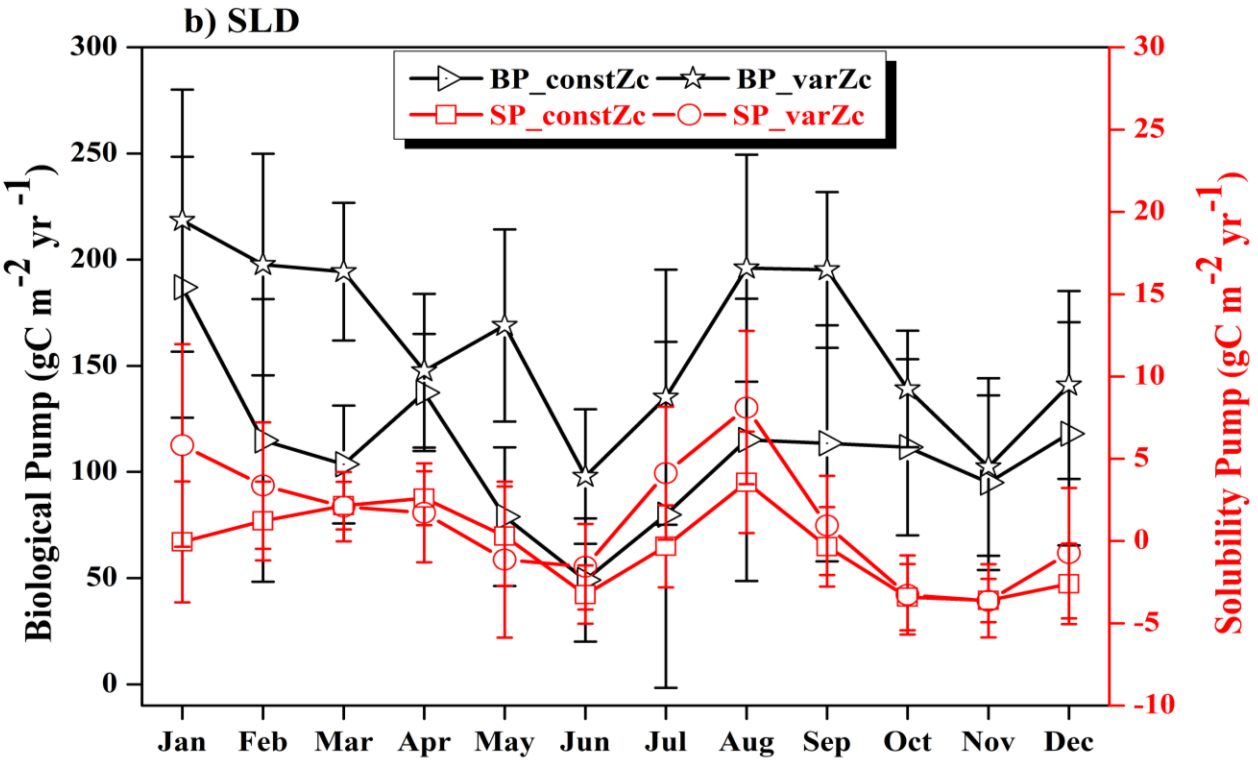
b) SLD
BP_constZc
BP_varZc
SP_constZc
SP_varZc
Biological Pump (gC m-2 yr-1)
Solubility Pump (gC m-2 yr-1)
0
50
100
150
200
250
300
-10
-5
0
5
10
15
20
25
30
Jan
Feb
Mar
Apr
May
Jun
Jul
Aug
Sep
Oct
Nov
Dec

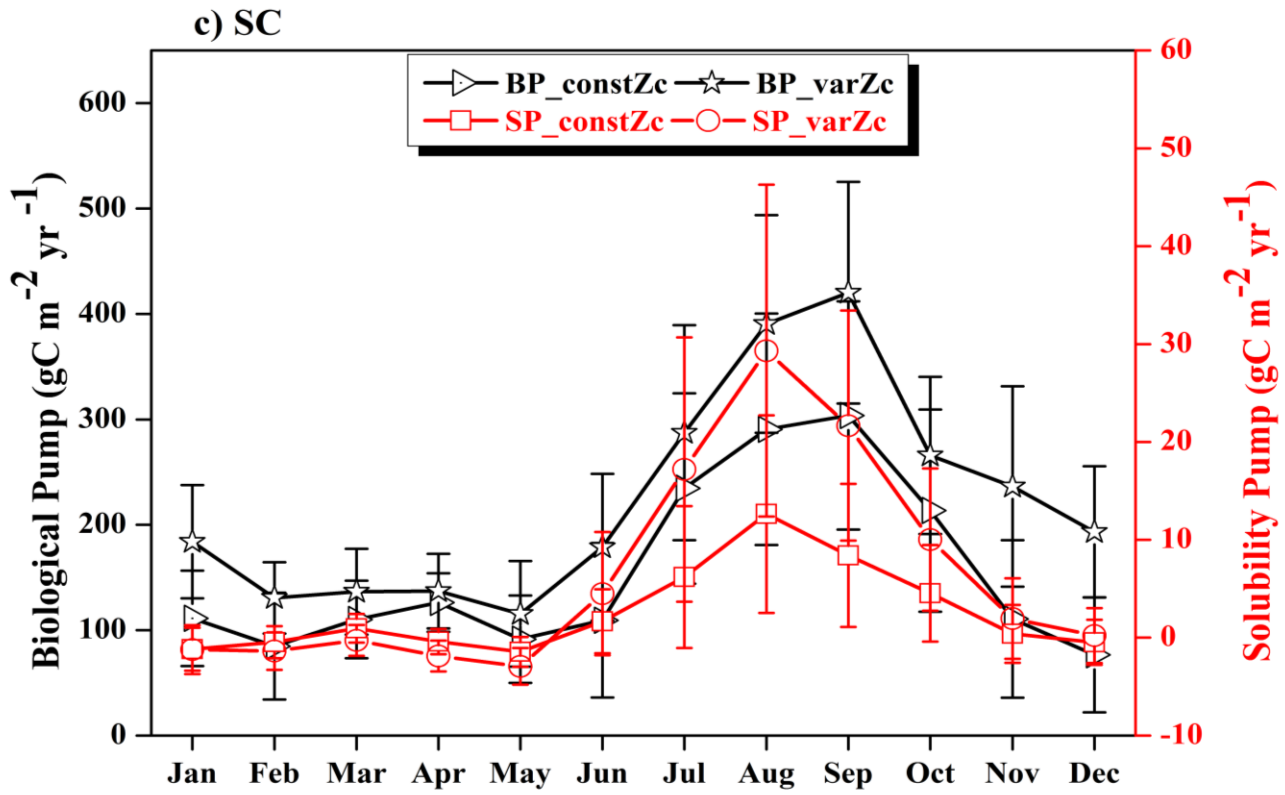
c) SC
BP_constZc
BP_varZc
SP_constZc
SP_varZc
Biological Pump (gC m-2 yr-1)
Solubility Pump (gC m-2 yr-1)
0
100
200
300
400
500
600
-10
0
10
20
30
40
50
60
Jan
Feb
Mar
Apr
May
Jun
Jul
Aug
Sep
Oct
Nov
Dec

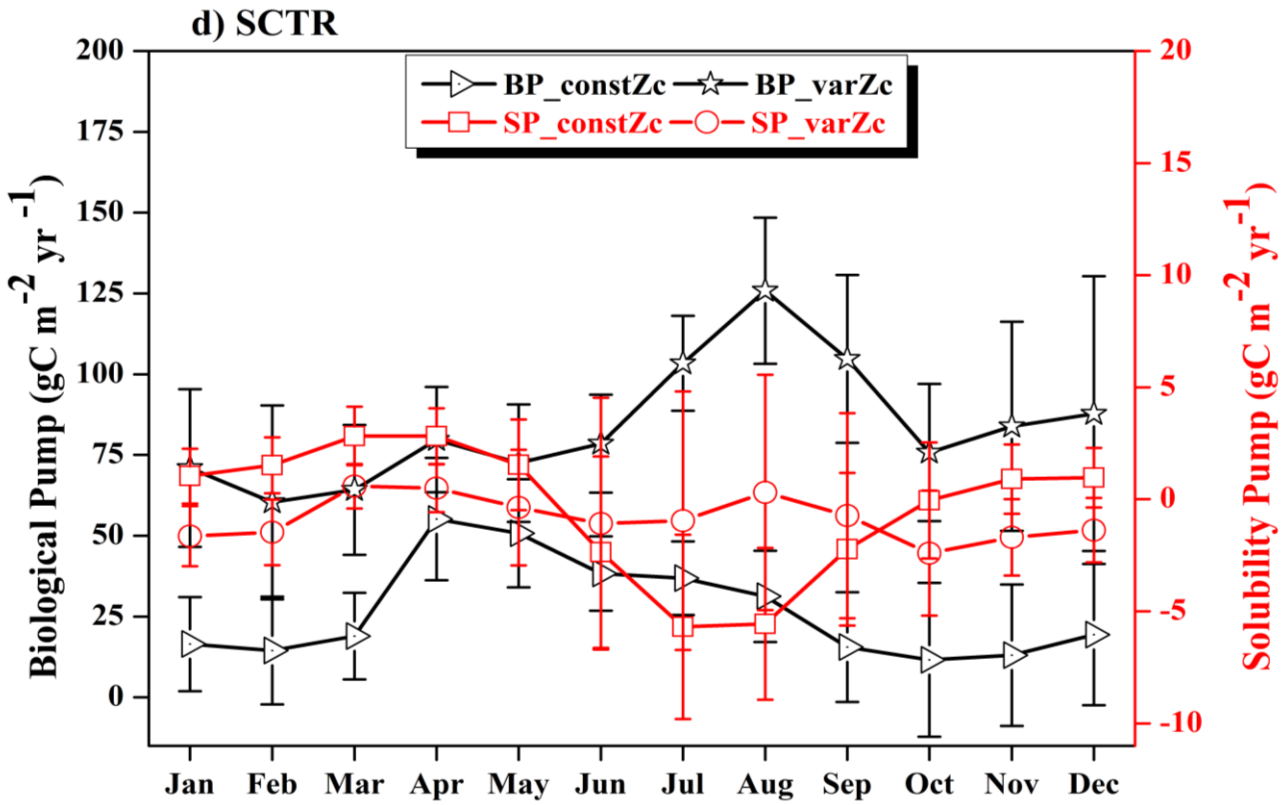

Figure 1(a-d): The strength of the biological pump (black lines) and solubility pump (red lines) as calculated based on Laounchi et al., (1996) equation (Eqs-1 and 2 above). The left axis shows the biological pump and the right axis shows the solubility pump. The units are in gC m^2 yr^{-1}.

Reply to the comments from Reviewer-2

Reviewer-2 offers very valuable comments especially for clarifying certain wording issues we had in the original manuscript. We sincerely thank the reviewer for enlightening us with the idea of "autotrophic compensation depth" which otherwise will not have been contrasted explicitly versus the community compensation depth. As per the definition from Marra et al., (2014) (thank you for pointing out this paper, this certainly clarified the wording issues we had), the autotrophic compensation depth is the depth where the gross primary production (GPP) balances the autotrophic respiration (R_a). In other words, it is the depth at which the Net Primary Production (NPP) equals zero. (ie. NPP = GPP – R_a). We admit that there were some wording issues in the original manuscript about the definition of compensation depth which created the confusion whether the compensation depth defined here is autotrophic compensation depth or community compensation depth, However, here we note that, the Ocean Carbon-cycle Model Intercomparison Project (OCMIP – II) protocol recommends the community compensation depth adapted from (Smetacek and Passow, 1990). According to this definition the community compensation depth is the depth at which the phytoplankton photosynthesis is great enough to balances the community respiration (i.e., both the autotrophic and heterotrophic respiration). At the community compensation depth, the Net Community Production (NCP) is zero. i.e., NCP = NPP - R_h (Marra et al., 2014; Regaudie-de-Gioux and Duarte, 2010; Gattuso et al., 2006). As per the OCMIP-II protocol we have to stick to the community compensation depth, as our intention here is to suggest a spatio-temporal variability to it through Compensation Irradiance (E_{com}). In this framework, E_{com} is again the minimum light irradiance at which phytoplankton photosynthesis is great enough to balance the community respiration and the depth at which the irradiance is equal to the compensation irradiance is referred as community compensation depth (Sarmiento and Gruber, 2006). Therefore there is absolutely no error in this hypothesis as per Sarmiento and Gruber, (2006) as well as Marra et al., (2014) and Regaudie-de-Gioux and Duarte, (2010). Again highlighting the definition of Regaudie-de-Gioux and Duarte (2010), the compensation irradiance for the community metabolism is the irradiance at which gross community primary production balances respiratory carbon losses for the **ENTIRE** community (Gattuso et al., 2006, Regaudie-de-Gioux and Duarte, 2010). This means that the OCMIP-II protocol assumes the compensation depth as the depth

where the gross primary production is equal to the community respiration. Therefore we are accurate in our definitions of compensation depth as per OCMIP-II protocol. At the same time we admit that in the original manuscript it was mentioned as 'compensation depth is the depth at which the photosynthesis equals planktonic respiration' (line-214). We corrected this error in the revised manuscript. Thank you.

With the literature survey suggested by Reviewer-2 we are now aware of the alternative definition and concept of autotrophic compensation depth and community compensation depth. However, the present study focuses on parameterizing the spatio-temporally varying compensation depth (i.e., **Community compensation depth** [Smetacek and Passow, 1990; Najjar and Orr, 1998]) as per the OCMIP –II protocol in order to quantify how it impacts the seasonal biases in the carbon cycle since biases were reported as a caveat in model simulations by Orr et al., (2003).

Another important point raised by Reviewer-2 is whether our choice of 10 w/m^2 cut-off as compensation irradiance (E_{com}) is justified when converted to mole photon/m^2/day. We argue that this choice is indeed justified especially in view of the following points.

1. Observations show that primary production reduces rapidly to 20% or less of the surface value below threshold of 10 W m^{-2} (Parsons et al., 1984; Ryther, 1956).
2. Higher ocean temperature (those in the tropics) enhances respiration rates resulting in high compensation irradiance (Parsons et al., 1984; Ryther, 1956; Lopez-Urrutia et al., 2006; Regaudie-de-Gioux and Duarte, 2010).
3. Table-1 of Regaudie-de-Gioux and Duarte, (2010) reports 0.4±0.2 mole photon/m2/day in case of Arabian Sea which is close to what 10 W m^{-2}.

We have revised the manuscript by taking into account all the comments by the reviewer. A point-by-point reply to reviewer's comment is as follows. For clarity the comments are shown in blue fonts.

1. Line 121. I disagree with citing "Sarmiento et. al. 2006." First, It should actually be "Sarmiento and Gruber. 2006" since that is the only citation for 2006. Sarmiento and Gruber is a book, with only one mention of the compensation depth; hardly justifying a

citation when there are whole contributions dealing with it (e.g., Marra et. al., 2014, DSR 83:45-50). Better would be Ryther, from L&O, 1956, but which in the references is listed as "2003."

We apologize for the citation error in the manuscript. We corrected the citations, Sarmiento and Gruber, (2006) and Ryther, (1956). As per your suggestion a literature review has been conducted on Marra et al., (2014) and further added discussions based on this paper. Please see Page-6, Line-115 and Page-12, Line 257 of the revised manuscript.

2. Line 120. They use the old symbol for irradiance. Use 'E'.

   Modified the symbol for compensation irradiance as 'E_{com}'.

3. Line 124: "Suppressed"? Not Suppressed, but the growth will be negative, phytoplankton will decline through respiration.

   Corrected as suggested. Please see Page-6, Line-113.

4. Line 125: Here is the crux of the matter. The authors continually confuse the community compensation depth with the autotrophic compensation depth. I have argued that the latter is more appropriate, since if autotrophic production is negative, the community compensation depth will be 0m: at the ocean's surface. The compensation irradiance is not where "planktonic photosynthesis" equals respiration, it is where GROSS photosynthesis = autotrophic respiration.

   It seems as if the authors want the community compensation depth (See papers Carlos Duarte, e.g.), and that's ok. They just have to define their parameters. Najjar and Keeling (1997), based on oxygen distributions can give only the community compensation depth.

   Responses to comment #4 and 5 are combined below.

5. Line 141: work in units of quanta, not energy. I've made the conversion and it appears that is equivalent to 1.7 mol photons/m2/d. or about 6% of the total daily surface

irradiance. For a community compensation irradiance, that might be ok, but I don't agree that that is the right parameter.

A better way to get the compensation depth is to use the base of the chlorophyll-a maximum as the bottom of the euphotic zone. There is justification for this experimentally (Marra et. al., 2014), and also intuitively, in that it captures all the autotrophic biomass. This of course is the autotrophic compensation depth, which I argue is better for modeling purposes than a community compensation depth.

Reply 4 & 5

Thank you for pointing out the wording confusion in the manuscript writing regarding the definition of compensation depth and educating us about the autotrophic compensation depth. We want to emphasize that we are parameterizing a **spatio-temporally varying compensation depth** in the OCMIP –II protocol which is **community compensation depth,** not autotrophic compensation depth. The definition is adopted as "the depth at which the phytoplankton photosynthesis is great enough to balance the community respiration or the depth at which compensation irradiance for community metabolism is satisfied [the irradiance at which gross community primary production balances respiratory carbon losses for the entire community] (Gattuso et al., 2006; Regaudie-de-Gioux and Duarte, 2010; Sarmiento and Gruber, 2006). As per the protocol of OCMIP-II we adopt the community compensation depth because of the following reasons:

(a) The OCMIP –II protocol defines it clearly as a community compensation depth above which is the production zone and below is the consumption zone (Najjar and Orr, 1998). And the OCMIP –II models are very successful in simulating the annual mean state of the carbon cycle. This also allows us a direct comparison with previous results.

(b) If we introduce the autotrophic compensation depth, which is depth at which photosynthesis is equal to autotrophic respiration, we will lose the contribution of inorganic carbon sources from the heterotrophic respiration (Regaudie-de-Gioux and

Duarte, 2010) and there is a possibility that this will affect the annual mean carbon cycle which is net effect of both autotrophic as well as heterotrophic respiration.

However we do agree that in the original manuscript there were confusions in the wording of our definitions, which we have revised. Please see Page-5, Line-106-110 and Page-11, Line-242-243.

6. Line 252: Again, there is a confusion about which compensation depth the authors are reffering to. My guess is that Smetacek and Passow (1990) are talking about the community compensation depth, whereas what is mentioned here is the autotrophic compensation depth.

   Corrected accordingly.

7. Line 262: Ryther (2003) ??
   The rest of the ms is the working out of the model results, which I can't really comment on. But the results all stem from the compensation depth. It is not clear to me whether the model currency is oxygen or carbon.

   Corrected Ryther (2003) as Ryther (1956).
   The model currency for OCMIP –II protocol is Phosphate and Dissolved Inorganic Carbon (Najjar and Orr, 1998).

References:

Gattuso, J. P., B. Gentili, C. M. Duarte, J. A. Kleypas, J. J. Middelburg, and D. Antoine.: Light availability in the coastal ocean: Impact on the distribution of benthic photosynthetic organisms and their contribution to primary production, Biogeosciences, 3, 489 – 513, doi: 10.5194/bg-3-489-2006, 2006.

Lopez-Urrutia, A., E. San Martin, R. P. Harris, and X. Irigoien.: Scaling the metabolic balance of the oceans, Proc. Natl. Acad. Sci. U.S.A., 103, 8739-8744,doi:10.1073/pnas.0601137103, 2006.

Marra, J. F., Veronica P. Lance, Robert D. Vaillancourt, Bruce R. Hargreaves.: Resolving the ocean's euphotic zone, Deep Sea. Res. pt. I., 83, 45 -50, doi:10.1016/j.dsr.2013.09.005, 2014.

Najjar, R. G., Orr, J. C.: Design of OCMIP-2 simulations of chlorofluorocarbons, the solubility pump and common biogeochemistry, http://www.ipsl.jussieu.fr/OCMIP/., 1998.

Orr, J. C., Aumont, O., Bopp, L., Calderia, K., Taylor, K., et. al.: Evaluation of seasonal air-sea CO2 fluxes in the global carbon cycle models, International open Science conference (Paris, 7-10 Jan. 2003), 2003.

Parsons, T. R., Takahashi, M., Habgrave, B.: In Biological Oceanographic Processes, 3rd ed., 330pp., Pergamon Press, New York, doi: 10.1002/iroh.19890740411, 1984

Regaudie-de-Gioux, A., and C. M. Duarte.: Compensation irradiance for planktonic community metabolism in the ocean, Global Biogeochem. Cycles, 24, GB4013, doi: 10.1029/2009GB003639, 2010.

Ryther, J. H.: Photosythesis in the ocean as a function of the light intensity, limnol. Oceanogr., 1, 61 -70, doi:10.4319/Io.1956.1.1.0061, 1956.

Sarmiento, J. L., and Gruber, N.: Ocean Biogeochemical Dynamics, Princeton University Press, New Jersey, 2006

Smetacek, V., and Passow, U.: Spring bloom initiation and Sverdrup's critical depth model, Limnol. Oceanogr., 35, 228 – 234, doi: 10.4319/lo.1990.35.1.0228, 1990.

Optimization of Biological Production for Indian Ocean upwelling zones: Part – I: Improving Biological Parameterization via a variable Compensation Depth

Mohanan Geethalekshmi Sreeush[1,2,*].

Vinu Valsala[1],

Sreenivas Pentakota[1],

Koneru Venkata Siva Rama Prasad[2],

Raghu Murtugudde[3]

[1]Indian Institute of Tropical Meteorology, Pune, India

[2]Department of Meteorology and Physical Oceanography, Andhra University, India

[3]ESSIC, University of Maryland, USA

(*Under revision BGD*)

*Corresponding author address:
Indian Institute of Tropical Meteorology,
Dr. Homibhabha Road, Pashan, Pune 411 008, India
E-Mail: sreeushmg@tropmet.res.in

Abstract

Biological modeling approach adopted by the Ocean Carbon Cycle Model Inter-comparison Project (OCMIP-II) provided amazingly simple but surprisingly accurate rendition of the annual mean carbon cycle for the global ocean. Nonetheless, OCMIP models are known to have seasonal biases which are typically attributed to their bulk parameterization of 'compensation depth'. Utilizing the principle of minimum solar radiation for the production and its attenuation by the surface Chl-a, we have proposed a new parameterization for a spatially and temporally varying 'compensation depth' which captures the seasonality in the production zone reasonably well. This new parameterization is shown to improve the seasonality of CO_2 fluxes, surface ocean pCO_2, biological export and new production in the major upwelling zones of the Indian Ocean. The seasonally varying compensation depth enriches the nutrient concentration in the upper ocean yielding more faithful biological exports which in turn leads to an accurate seasonality in carbon cycle. The export production strengthens by ~70% over western Arabian sea during monsoon period and achieved a good balance between export and new production in the model. This underscores the importance of having a seasonal balance in model export and new production for a better representation of the seasonality of carbon cycle over upwelling regions. The study also implies that both the biological and solubility pumps play an important role in the Indian Ocean upwelling zones.

Keywords: Indian Ocean upwelling zones, Carbon cycle, Seasonal cycle - CO_2 flux and Oceanic pCO_2, Biogeochemical model parameterization, Export production - New production balance, Solubility and Biological pump.

1. Introduction

~~Among the world's oceans,~~ Indian Ocean is characterized ~~with~~ by the ~~a~~ unique seasonally reversing monsoon wind systems which act as ~~called monsoon winds,. The monsoon winds are~~ the major physical drivers for the coastal and open ocean upwelling processes.~~ in the Indian Ocean~~. The major upwelling systems in the Indian Ocean are (1) the western Arabian Sea (WAS; Ryther et. al., 1965, Smith et. al., 2001, Sarma., 2004, Wiggert et. al., 2006, Murtugudde et. al., 2007, McCreary et. al., 2009, Prasanna Kumar et. al., 2010, Naqvi et. al., 2010, Roxy et al., 2015) (2) the Sri Lanka Dome (SLD;Vinayachandran et al., 1998, 2004), (3) Java and Sumatra coasts (SC; Murtugudde et al., 1999, Susanto et. al., 2001, Osawa et. al., 2010, Xing et. al., 2012) and (4) the Seychelles-Chagos thermocline ridge (SCTR; Murtugudde et al., 1999; Dilmahamod., 2016, Figure 1). The physical and biological processes and their variability over these key regions are inseparably tied to the strength of the monsoon winds and associated nutrient dynamics. The production and its variability ~~in the~~ over these coastal upwelling systems are a key concern ~~to~~for the fishing community, since they affect the day-to-day livelihood of the coastal populations (Harvell et. al., 1999, Roxy et. al., 2015, Praveen et al., 2016)~~. Coastal upwelling systems account for about 11% of the world oceanic biological production (Prasanna Kumar et al., 2001, Wiggert et al., 2005, Levy et al., 2007, McCreary et al., 2009, Liao et. al., 2016)~~ and are ~~especially~~ important for the Indian Ocean rim countries due to their developing country status.

Arabian Sea is a highly productive coastal upwelling system characterized by phytoplankton blooms both in summer (Prasanna Kumar et al., 2001, Naqvi et al., 2003, Wiggert et al., 2005) and winter (Banse K. et. al., 1986, Schubert et. al., 1998, Wiggert et. al., 2000, Barber et. al., 2001, Prasannakumar et al., 2001, Sarma., 2004). Arabian Sea is known for the second largest

Tuna fishing region in the Indian Ocean ~~among all oceans~~ (Lee et al., 2005). The Somali and Omani upwelling regions experience phytoplankton blooms that are prominent with Net Primary Production (NPP) exceeding ~~438.29~~435 g C m^{-2} yr^{-1} (Liao et. al., 2016). On the other hand productivity over the SLD (Vinayachandran and Yamagata, 1998), in the sea of Sri Lanka is triggered by an open ocean Ekman suction~~. SLD shows~~ with strong Chl-a blooms during the summer monsoon (Murtugudde et al., 1999, Vinayachandran et al., 2004). ~~Compared to the Arabian Sea this bloom lasts for more than four months due to the impact of biogeochemistry of the region (Vinayachandran et. al., 2004). During the winter monsoon, the southwest Bay of Bengal is also characterized by Chl-a blooms associated with the intense cyclonic activities (Vinayachandran and Mathew, 2003).~~ Similarly the SC upwelling is basically due to the stronger alongshore winds and its variation is associated with impact of equatorial and coastal Kelvin waves (Murtugudde et. al., 2000). The interannual variability associated with the Java-Sumatra coastal upwelling is strongly coupled with ENSO (El-Niño Southern Oscillation) through the Walker cell and Indonesian throughflow (Susanto. et. al., 2001, Valsala et al., 2011) and peaks in July through August with a potential new production of 0.1 Pg C yr^{-1} (Xing et. al., 2012). The SCTR ~~region~~ productivity has a large spatial and interannual variability. The warmer upper ocean condition associated with El Niñ~~n~~o reduces the amplitude of ~~the~~ subseasonal SST variability over the SCTR (Jung and Kirtman., 2016). The Chl-a concentration peaks in summer when the southeast trade winds induce mixing and initiate the upwelling of nutrient-rich water (Murtugudde et. al., 1999, Wiggert et al., 2006, Vialard. J. et. al., 2009, Dilmahamod et al., 2016).

Understanding the biological production and variability in the upwelling systems ~~are~~ is important because it gives us crucial information regarding marine ~~species~~ecosystem variability

(Colwell, 1996, Harvell et al., 1999). The observations also provide vital insights into physical and biological interactions of the ecosystem (Naqvi et al., 2010) as well as the biophysical feedbacks (Murtugudde et al., 2001) although limitations of sparse observations often force us to depend on models to examine the large spatio-temporal variability of the ecosystem (Valsala et al., 2013). Simple to inter-mediate complex marine ecosystem models have been employed by several of the previous studies (Sarmiento et. al., 2000, Orr. et. al., 2001, Matsumoto et. al., 2008). However the representation of marine ecosystem ~~variability by~~ with proper parameterizations in models has always been a daunting task. This is an impediment to the accurate representation of biological primary and export productions in models (Friedrichs et al., 2006, 2007) and these ~~parameterization~~ issues also impact the modeling of upper trophics levels (Lehodey et al., 2010).

Biological production can be quantified with a better understanding of primary production ~~by phytoplankton. Primary production~~ which depends on water temperature, light and nutrient availability (Brock. et. al., 1993, Moisan et. al., 2002) and this became the key reason for parameterizing the production in models as one or more combinations of these terms (Yamanaka et. al., 2004). Any of these basic parameters can be tweaked to alter production in models. For example the availability of nutrients and light determines the phytoplankton growth (Eppely et al., 1972) or growth rate (Boyd et. al., 2013). Stoichiometry and carbon-to-Chl-a ratios are other important factors to be considered in modeling (Christian et al., 2001, Wang et al., 2009) but we will not consider them in this study.

~~In 1995, an initiative by the IGBP/GAIM (International Geosphere Biosphere program/Global Analysis, Integration and Modeling) and IGBP/JGOFS (Joint Global Ocean Flux Study) to study carbon cycle referred to as~~ The Ocean Carbon cycle Model Intercomparison

Project (OCMIP) greatly improved our understanding of global carbon cycle (~~Raymond~~ Najjar and ~~James~~ Orr, 1998). OCMIP-II further introduced a simple phosphate dependent production term in biological models for long term simulations of carbon cycle in response to anthropogenic climate change with an accurate annual mean state (Najjar et al, 1998, Orr et al., 2001, Doney et. al., 2004). ~~Although OCMIP – II is a very simplified model, it is surprisingly accurate in simulating the annual mean state and the response to anthropogenic climate change (Orr et al., 2001, Doney et. al., 2004).~~ However, the OCMIP – II model simulations comes with a penalty of higher seasonal biases when compared with observations (Orr et al., 2003). In this protocol the light limitation is formulated as a bulk quantity with the notion that the minimum light irradiance at which phytoplankton photosynthesis is sufficient to balance the community respiration, E_{com}, is the compensation irradiance (Sarmiento and Gruber, 2006) and the depth at which the phytoplankton photosynthesis equals whole community respiration is the community compensation depth Zc (Smetacek and Passow, 1990, Gattuso et. al., 2006, Regaudix-de-Gioux and Duarte, 2010, Marra et. al., 2014), Note that Zc is ~~which is~~ clearly different from the conventional euphotic zone depth (Morel., 1988). If the irradiance is ~~below~~ less than E_{com}, the growth will be negative, phytoplankton will decline through respiration. If the irradiance is ~~above this~~ larger than E_{com}, the planktonic photosynthesis will exceed the community respiration and production will increase (Parsons et. al., 1984, Sarmiento and Gruber, 2006). Therefore the compensation depth represents the oceanic production zone in this approach. However, Zc was held constant in time and space in OCMIP-II models (~~Raymond~~ Najjar and ~~James~~ Orr, 1998, Matsumoto et. al., 2008) though in reality Zc varies in space and time (Najjar and Keeling, 1997) just as the euphotic zone depth does as documented in ship measurements (Qasim, 1977, 1982). The variation in compensation depth indicates the seasonality of the production zone

itself. ~~Availability of light and nutrients at an optimum level is clearly essential for primary production.~~

Most of the biophysical models prescribe a constant value for compensation depth (e.g., Zc = 75m in OCMIP –II protocol (Najjar and Orr, 1998), Zc = 100m for Minnestoa Earth System Model (Matsumoto et. al., 2008) ~~although in reality it is not a constant.~~ Depending on the latitude, compensation depth varies between 50m and 100m in the real world (Najjar and Keeling, 1997). In our study we have attempted a novel biological parameterization scheme for spatially and temporally varying community compensation depth in the OCMIP–II framework by representing it as a function of optimum solar radiation (Parsons et. al., 1984) and Chl-a availability. In this hypothesis, the compensation irradiance is taken as 10 W m^{-2} and calculated its depth from a Chl-a attinueated solar radiation inorder to yield spatially and temporally varying Zc. ~~the minimum solar radiation required for photosynthesis is taken as 10 W m^{-2} below which the production reduces to 20% (Parsons et. al., 1984) and the Chl-a concentration which determines the attenuation of solar radiation with depth in the production zone is also assumed to vary to yield the spatio-temporal variability of Zc. The basic currency of phosphate will act as limiting factor for~~ Phosphate is the basic currency which limits biological production within this varying compensation depth. This spatially and temporally varying compensation depth represents the seasonality in the production zone which is lacking originally in OCMIP-II.

Regions of sustained upwelling like the eastern equatorial Pacific are well understood in terms of the role of upwelling in increasing the surface water pCO_2 to drive an outgassing of CO_2 into the atmosphere (Feely et al., 1999, Valsala et al., 2014). The Indian Ocean on the other hand only experiences seasonal upwelling which is relatively weak in the deep tropics but stronger off the coasts of Somalia and Oman and in the SLD ~~region~~ (Valsala et al., 2013). The relative

importance of the solubility vs. biological pump is not well understood. Our focus here on implementing seasonality in the compensation depth of OCMIP models nonetheless leads to new insights on the impact of improved biological production on surface water pCO_2 and air-sea CO_2 fluxes. The largely positive effects of the variable compensation depth over the Indian Ocean and the sensitivity experiments where upwelling is muted strongly imply that the biological pump may play as much of role as the solubility pump in determining surface pCO_2 and CO_2 fluxes over the Indian Ocean.

The paper is organized as follows. Model, Data and Methods~~ology~~ are detailed in Section 2. The spatially inhomogeneous Zc derived out of the new parameterization and its impact in simulated seasonality of biology and carbon cycle are detailed in Section 3. Further results and discussion are followed in Section 4 and a conclusion is given in Section 5.

2. Model, Data and Methods

2.1. Model

The study utilizes the Offline Ocean Tracer Transport Model (OTTM~~);~~ ~~(~~Valsala et al., 2008) coupled with OCMIP biogeochemistry model (~~Raymond~~ Najjar and~~ James~~ Orr, 1998). OTTM does not compute currents and stratifications (i.e., temperature and salinity) on its own. It is capable of accepting any ocean model or data-assimilated product as physical drivers. The physical drivers prescribed include 4-dimensional currents (u,v), temperature, salinity, and 3-dimensional mixed layer depth, surface freshwater and heat fluxes, surface wind stress and sea surface height. The resolution of the model setup is similar to the parent model from which it borrows the physical drivers. With the given input of Geophysical Fluid Dynamics Laboratory (GFDL) reanalysis data, the zonal and meridional resolutions are 1^o with 360 grid points

longitudinally and 1^{o} at higher latitudes but having a finer resolution of 0.8^{o} in the tropics, with 200 latitudinal grid points, respectively. The model has 50 vertical levels with 10m increment in the upper 225m and stretched vertical levels below 225m. The horizontal grids are formulated in spherical co-ordinates and vertical grids are in z levels. The model employs a B-grid structure in which the velocities are resolved at corners of the tracer grids. The model uses a centered-in-space and centered-in-time (CSCT) numerical scheme along with an Asselin-Robert filter (Asselin., 1972) to control the ripples in CSCT.

The tracer concentration (C) evolves with time as

$$\frac{\partial C}{\partial t} + U.\nabla_H C + W\frac{\partial C}{\partial z} = \frac{\partial}{\partial z}K_z\frac{\partial}{\partial z}C + \nabla_H.(K_h\nabla_H C) + \Phi \qquad (1)$$

where ∇_H is the horizontal gradient operator, U and W are the horizontal and vertical velocities respectively. K_z is the vertical mixing coefficient, and K_h is the two-dimensional diffusion tensor. Φ represents any sink or source due to the internal consumption or production of the tracer as well as the emission or absorption of fluxes at the ocean surface. Here, the source and sink term are provided through the biogeochemical model. Vertical mixing is resolved in the model using K- profile parameterization (KPP) (Large et al., 1994).

In addition to KPP, the model uses a background vertical diffusion reported by Bryan and Lewis (Bryan and Lewis., 1979) ~~in order to represent the convention and mixing that happens in a time scale of a few days.~~ For horizontal mixing model incorporates Redi fluxes (Redi., 1982) and GM fluxes (Gent and Mcwilliams., 1990) which ~~accommodate~~ represent the eddy-induced variance ~~from~~in the mean in the tracer transport. A weak Laplacian diffusion is also included in the model for computational stability where sharp gradient ~~of~~in concentration occurs.

The biogeochemical model used in the study is based on the OCMIP – II protocol as stated above. The main motivation of OCMIP–II model design is to simulate the ocean carbon cycle with ~~reductionist~~ restoration approach to ocean biology using appropriate biogeochemical parameterizations. The major advantage of the OCMIP – II protocol is (i) it reproduces the first order carbon cycle and the associated elemental cycles in the ocean reasonably well and (ii) it is much easier to implement and computationally efficient than the explicit ecosystem models. The present version of the model has five prognostic variables coupled with the circulation field, viz., inorganic phosphate (PO_4^{3-}), dissolved organic phosphorous (DOP), oxygen (O_2), dissolved inorganic carbon (DIC) and alkalinity (ALK). In order to retrieve the accurate spatial and temporal distribution of CO_2 flux and pCO_2, the model uses a "nutrient restoring" approach (Najjar et. al., 1992, Anderson and Sarmiento., 1995) for biological production. The basic currency for biological production in the model is phosphate because of the availability of a more extensive database and to eliminate the complexities associated with nitrogen fixation and denitrification. The biogeochemical dynamics implemented in the model and the calculations of solubility and biological pump are ~~given~~ provided in Appendix-A

The air – sea CO_2 flux in the model is estimated by,

$$F = K_w \, \Delta \, pCO_2 \qquad (2)$$

where K_w is gas transfer velocity and $\Delta \, pCO_2$ is the difference in partial pressure of carbon dioxide between the ocean and atmosphere. The design and validation of the physical model is reported by Valsala et. al.,(2008, 2010) and biogeochemical design by Najjar and Orr (1998).

2.2. Data

The present setup of the model uses ocean reanalysis products based on MOM–4 (Modular Ocean Model) developed by GFDL (Chang et. al., 2012). Monthly data from 1961 to 2010 were utilized in the present study. For validating the results observational datasets of CO_2 flux and pCO_2 were taken from Takahashi et al., (2009). Satellite derived Net Primary Production data were taken from Sea-viewing Wide Field of view sensor (SeaWiFS) Chl-a product, calculated using Vertically Generalized Production Model (VGPM) (Behrenfeld and Falkowski, 1997). The initial conditions for PO_4 and O_2 were taken from World Ocean Atlas ~~(Conkright et al., 1994)~~ (Garcia et al., 2014). Initial conditions for DIC and ALK were taken from the Global Ocean Data Analysis Project (GLODAP; Key et al., 2004) dataset. The data sources and citations are ~~given~~ provided in the Acknowledgement.

2.3. Methods

A spin-up for 50 years from the given initial conditions ~~are~~is performed with the climatological physical drivers. Because the initial conditions were provided from a mean state observed climatology this duration of spin-up is sufficient to reach statistical equilibrium in the upper 1000 m (Le Quere et al., 2000). Atmospheric pCO_2 has been set to a value from the 1950s in the spin-up run for calculating the air-sea CO_2 exchange. A seasonal cycle of atmospheric pCO_2 has been prescribed.

After the spin-up, an interannual simulation for 50 years from 1961 to 2010 has been carried out with the corresponding observed atmospheric pCO_2 described in Keeling et al, (1995). The first five years of the interannual run were looped five times through the physical fields of 1961 repeatedly for a smooth merging of the spin-up restart to the interannual physical variables. Since the study is focused only on bias corrections to the seasonal cycle with a

variable Zc, a model climatology has been constructed from 1990 to 2010. This includes the anthropogenic increase of oceanic DIC in the climatological calculation and is comparable with the Takahashi et al. (2009) observations.

Additional two sensitivity experiments have been performed separately by providing annual mean currents or temperatures as drivers over selected regions of the basin for segregating the role of varying compensation depth (varZc) in improving the seasonality of carbon cycle and biological production. The model driven with annual mean currents suppress the effect of upwelling by muting the Eekman divergence over the region of interest. On the other hand, the model forced with annual mean temperatures suppresses the cooling effect of upwelling. This will highlight the effect of new parameterization in simulating seasonality of carbon cycle and biological production. A smoothing technique with linear interpolation ($u = u(1-x) + \bar{u}x$) is applied to the offline-data in order to blend the annual mean fields ($\bar{u}$) ~~given~~provided to the selected region with the rest of the domain (u) ~~in order~~ to reduce ~~a~~ the sudden transition at the boundaries.

2.4. Community Compensation depth (Z_c) parameterization

The OCMIP – II ~~simulation~~ protocol separates the production and consumption zones by a depth termed as compensation depth (Z_c); the depth at which phytoplankton photosynthesis is large enough to balance the community respiration (i.e., both the autotrophic and heterotrophic respiration). At the community compensation depth, the Net Community Production (NCP) is zero i.e., NCP = NPP - R_h = 0, where NPP is Net Primary Production (i.e. NPP = GPP – $R_{a)}$, GPP is gross primary production, and R_h and Ra are the heterotrophic and autotrophic respirations, respectively (Smetacek and Passow., 1990, Najjar and Orr, 1998, Gattuso et. al.,

2006, Regaudix-de-Gioux and Duarte, 2010, Marra et. al., 2014). ~~the depth at which photosynthesis is equal to respiration of the photosynthetic community (Smetacek and Passow., 1990).~~ The light intensity at compensation depth is compensation irradiance (E_{com}), the irradiance at which the gross community primary production balances respiratory carbon losses for the entire community (Gattuso et. al., 2006, Regaudix-de-Gioux and Duarte, 2010). ~~(I_c) with larger values at higher temperatures since respiration is temperature dependent (Parsons et. al., 1984, Ryther, 1956).~~ We define a spatially and temporally varying compensation depth (hereinafter varZc) as a depth where compensation irradience (attenuated by surface Chl-a, Jerlov et al., 1976) reaches a minimum value of 10 W m^{-2}. In this way the varZc has both spatio-temporal variability of light as well as Chl-a ~~data~~. The Chl-a is given as monthly climatology as constructed from the satellite data. Observations show that the primary production reduces rapidly to 20% or less of the surface value below a threshold of 10 W m^{-2} (Parsons et.al., 1984, Ryther, 1956, Sarmiento and Gruber, 2006). Moreover higher ocean temperature (those in the tropics) enhances the respiration rates resulting in high compensation irradiance (Parsons et. al., 1984, Ryther, 1956, Lopez-Urrutia et. al., 2006, Regaudix-de-Gioux and Duarte, 2010). A study by Regaudix-de-Gioux and Duarte (2010) reported the mean value of compensation irradiance of Arabian Sea as 0.4 ± 0.2 mol photon m^{-2} day^{-1} which is close to 10 W m^{-2} day^{-1}.

Figure 2 compares the scatter of average relative photosynthesis within varZc as a function of solar radiation for the Indian Ocean. This encapsulate the corresponding curve from the observations for the major phytoplankton species in the ocean such as diatoms, green algae and dinoflagellates (Ryther et al., 1956, Parsons et al., 1984, Sarmiento and Gruber, 2006). The model permits 100% relative photosynthesis for radiation above 50 W m^{-2}. However the availability of phosphate concentration in the model act as an additional limiter for production

which indirectly represents the photoinhibition at higher irradiance, for example oligotrophic gyres.

3. **Results and Discussions**

The inclusion of seasonality in Zc by way of parameterizing varZc leads to a remarkable spatio-temporal variability in compensation depth (Figure 3). The compensation depth over the Arabian Sea varies from 10m to 25m during December to February (DJF) and deepens up to 45m during March to May (MAM) in par with incoming solar radiation. During the monsoon season i.e., June to September (JJAS), the compensation depth again shoals to 10m-35m due to the attenuation of solar radiation by the increased biological production (Chl-a). During October to November (OCT-NOV) the Zc slightly deepens as compared to JJAS.

The Bay of Bengal compensation depth deepens from 35m to 40m during DJF and further deepens to 50m during MAM when the solar radiation is maximum and biological production is minimum (Prasannakumar et al., 2002). Further reduction of compensation depth can be seen through JJAS as a result of reduction in solar radiation during monsoon cloud cover. The Zc during Oct – Nov is 35m on ~~an~~ average ~~of 35m~~. However, caution is needed since the Bay of Bengal is dominated by freshwater forcing from rivers and precipitation and temperature inversions occur routinely (Howden and Murtugudde., 2001, Vinayachandran et. al., 2013). The impact of these factors on compensation depth variability is not clear and is not addressed here.

The equatorial Indian Ocean can be seen as a belt of 40m-45m ~~deep~~ compensation depths throughout the season except for JJAS. During JJAS, a shallow compensation depth is seen near the coastal Arabian Sea (around 10m to 35m) presumably due to the coastal Chl-a blooms. Deep

compensation depth off the coast of Sumatra (~ 40m to 50m) is found during JJAS. Java-Sumatra coastal upwelling is centered on September to November (Susanto et al., 2001) and upwelling originates at around 100m deep (Valsala and Maksyutov, 2010; Xing et al., 2012).

Southward of 10°S in the oligotrophic gyre region, the compensation depth varies from 40m to more than 60m throughout the year. A conspicuous feature observed while parameterizing the solar radiation and Chl-a dependent Zc is that its maximum value never crosses 75 m especially in the Indian Ocean which is the value specified in OCMIP-II models. The cutoff depth of 75 m in OCMIP-II is obtained from observing the seasonal variance in the oxygen data (Najjar and Keeling, 1997) as an indicator of production zone. However, our results show that parameterizing a production zone based on optimum solar radiation and Chl-a (Parsons et al., 1984) predicts a production zone and its variability that is largely less than 75 m. The consequence of this in the seasonality of the modeled carbon cycle is illustrated as follows.

3.1. Simulated seasonal cycle of pCO_2 and CO_2 fluxes

The annual mean biases in simulated CO_2 fluxes and pCO_2 were evaluated by comparing with Takahashi et al., (2009) observations (Figure 4). The model biases are significantly reduced with the implementation of varying Z_c compared to that of the constant Z_c. A notable reduction in pCO_2 bias (by ~ 10µatm) is observed along the WAS region [Figure (4d)].

In order to address the role of the new biological parameterization of a variable compensation depth, we extended our study by choosing four key regions where the biological production and CO_2 fluxes are prominent in the Indian Ocean with additional sensitivity experiments (see Introduction and references therein). The boxes we considered are, (1) Western Arabian Sea (WAS~~)~~ ~~[~~; 40°E:65°E, 5°S:25°N~~]~~) (2) Sri Lanka Dome (SLD~~)~~ ~~[~~; 81°E:90°E, 0°:10°N~~]~~)

(3) Seychelles-Chagos Thermocline Ridge (SCTR~~;) [~~50°E:80°E, 5°S:10°S~~]~~) and (4) Sumatra Coast (SC~~) [~~; 90°E:110°E, 0°:10°S; Figure 1~~]~~). The seasonal variations of Zc over these selected key regions are shown in Figure 5. A detailed analysis of CO_2 fluxes, pCO_2, biological export and new production and the impact of varZc simulations in improving the strength of biological pump and solubility pump for these key regions are presented below.

3.2. Western Arabian Sea (WAS) ~~region~~

The WAS Zc has a double peak pattern over the annual cycle. Over the February-March period Z_c deepens up to a maximum of 43.85 ± 2.3 m into March and then shoals to 25.75 ± 1.5 m (Fig 5) during the monsoon period (uncertainty represents the interannual standard deviations of monthly data from 1990-2010). This shoaling of compensation depth during the monsoon indicates the potential ability of the present biological parameterization to capture the wind driven upwelling related production in the WAS. During the post monsoon period, the second deepening of compensation depth occurs during November with a maximum depth of 34.91 ± 2.2 m. The ability to represent the seasonality of biological production zone renders a unique improvement in CO_2 flux variability especially in the WAS region in comparison to the OCMIP-II experiments (Orr et al, 2003, Figure (6a)).

OCMIP –II simulations with a constant Z_c of 75 m underestimate the CO_2 flux when compared to the observations of Takahashi et al. (2009). This underestimation is clearly visible during monsoon period. Our simulations with ~~the present biological parameterization having a spatially and temporally varying compensation depth~~ variable Zc result~~s~~ in a better seasonality of CO_2 flux when compared with Takahashi et al. (2009) observations (Figure 6a). The

358 improvement brought about by the ~~varying~~ variable Zc scheme is able to represent the
359 seasonality of CO_2 flux especially during the monsoon period, when wind driven upwelling is
360 dominant. Obviously the relative role of the biological and solubility pumps have to be
361 deciphered in this context.

362 The CO_2 flux during July from observations, constZc ~~simulations~~ and varZc simulations are
363 3.09 mol m^{-2} yr^{-1}, 1.82 ± 0.4 mol m^{-2} yr^{-1} and 3.10 ± 0.5 mol m^{-2} yr^{-1}, respectively. Southwesterly
364 wind-driven upwelling over the WAS especially off the Somali coast (Smith & Codispoti, 1980,
365 Schott, 1983, Smith, 1984) and Oman (Bruce, 1974, Smith &Bottero, 1977, Swallow, 1984,
366 Bauer et al, 1991), pulls nutrient-rich subsurface waters closer to the surface while the available
367 turbulent energy due to the strong winds leads to mixed layer entrainment of the nutrients
368 resulting in a strong surface phytoplankton bloom (Krey & Babenerd, 1976, Banse, 1987, Bauer,
369 1991, Brock et al, 1991). This regional bloom extends over 700 km offshore from the Omani
370 coast due to upward Ekman pumping driven by strong, positive wind-stress curl to the northwest
371 of the low level jet axis and the offshore advection (Bauer et. al., 1991, Brock et al., 1991, Brock
372 & McClain, 1992a, b, Murtugudde and Busalacchi., 1999; Valsala, 2009) resulting in strong
373 outgassing of CO_2 flux and an enhanced pCO_2 in the western Arabian Sea region (Valsala and
374 Maksyutov, 2013, Sarma et al., 2002). The seasonal mean CO_2 flux during the southwest
375 monsoon period (JJAS) for constZc ~~simulations~~ and varZc simulations are 1.44 ± 0.2 mol m^{-2} yr^{-1}
376 and 2.31 ± 0.4 mol m^{-2} yr^{-1}, respectively. The biological parameterization of varying
377 compensation depth considerably improves the average CO_2 flux during the monsoon period by
378 0.86 ± 0.1 mol m^{-2} yr^{-1}. The annual mean CO_2 flux from observations, constZc ~~simulations~~ and
379 varZc simulations are 0.94 mol m^{-2} yr^{-1}, 0.80 ± 0.17 mol m^{-2} yr^{-1} and 1.07 ± 0.2 mol m^{-2} yr^{-1},
380 respectively. The annual mean CO_2 flux improved by 0.27 ± 0.05 mol m^{-2} yr^{-1}.

Seasonality in pCO_2 also shows a remarkable improvement during the southwest monsoon period ~~[~~(Figure ~~(~~6b)~~]~~. The pCO_2 with ConstZc is considerably lower at a value of 385.22 ± 3.5 µatm during June compared to observational values of 392.83 µatm. However, varZc simulations perform better in terms of pCO_2 variability. The peak value of pCO_2 reaches up to 405.42 ± 5.8 µatm. The seasonal mean pCO_2 during the southwest monsoon period from observations, constZc ~~simulations~~ and varZc simulations are 397.58 µatm, 389.18 ± 3.6 µatm and 399.95 ± 5.0 µatm, respectively. The improvement in pCO_2 brought about by varZc simulations is 10.76 ± 1.3 µatm compared to the constZc simulations. This inherently says that constZc simulations fail to capture the pCO_2 driven by upwelling during the Southwest monsoon, meanwhile varZc simulations are demonstrably better in representing this seasonal increase. The annual mean pCO_2 from observations, constZc and varZc simulations are 394.69 µatm, 389.62 ± 3.9 µatm and 391.19 ± 4.7 µatm, respectively. However it is worth mentioning that there are parts of the year where the constant Zc performs better compared to varying Zc. For instance during MAM as well as in November, the constZc simulations yielded a better comparison with the observed pCO_2 whereas varZc simulations yield a reduced magnitude of pCO_2. This may well indicate the biological vs solubility pump controls on pCO_2 during the intermonsoons. The role of mesoscale variability in the ocean dynamics may also play a role (Valsala and Murtugudde, 2015) Nevertheless during the most important season (JJAS) when the pCO_2, CO_2 fluxes and biological production are found to be dominant in the Arabian Sea, the varying Zc produces a better simulation.

The improvement shown by the implementation of new biological parameterization in the simulations of CO_2 flux and pCO_2 can be ~~answered~~ elicited by further analysis of the model biological production. Figure 7 shows the comparison of model export production and new

production with observational export production from satellite-derived NPP for constZc and varZc simulations. The model export production in the constZc simulations is much weaker when compared to varZc simulations. The varZc simulations have improved the model export production. Theoretically, the new and export productions in the model should be in balance with each other (Eppley and Peterson, 1979). ConstZc export production is much weaker than new production and it is not in balance. In contrast the varZc simulation yields a nice balance among them.

Comparing with the observational export production which peaks in August at a value of 154.78 g C m^{-2} yr^{-1}, the varZc simulated export and new productions peak at a value of 160.44 ± 20.4 g C m^{-2} yr^{-1} and 167.18 ± 24.0 g C m^{-2} yr^{-1}, respectively but in July. A similar peak can be observed in constZc simulated new production as well at a value of 178.19 ± 28.0 g C m^{-2} yr^{-1}. This apparent shift of one month during JJAS in the model export production as well as in the new production is noted as a caveat in the present set up which will need further investigation. Arabian Sea production is not just limited by nutrients but also the dust inputs (Wiggert and Murtugudde., 2006). The dust induced primary production in the WAS especially over the Oman coast is noted during August (Liao et. al., 2016). The mesoscale variability in the circulation and its impact on production and carbon cycle are also a limiting factor in this model as noted above.

The seasonal mean export production during the Southwest monsoon period from satellite-derived estimate is 123.57 g C m^{-2} yr^{-1}, whereas for constZc and varZc simulations it is 84.81 ± 16.0 g C m^{-2} yr^{-1} and 147.19 ± 23.8 g C m^{-2} yr^{-1}, respectively. The new biological parameterization strengthen~~sed~~ the model export production by 62.38 ± 7.8 g C m^{-2} yr^{-1} for the Southwest monsoon period, which is over a 70% increase. This indicates a considerable impact of the biological pump in the model simulated CO_2 flux and pCO_2 over the WAS. For constZc

simulations, the computed new production is slightly higher (150.84 ± 27.9 g C m^{-2} yr^{-1}) than that of varZc (133.03 ± 19.5 g C m^{-2} yr^{-1}). The annual mean export production from observations, constZc and varZc simulations are 94.31 g C m^{-2} yr^{-1}, 77.41 ± 15.1 g C m^{-2} yr^{-1} and 122.54 ± 25.2 g C m^{-2} yr^{-1}, respectively.

To understand how the varying compensation depth parameterization strengthen~~sed~~ the export production in the model, we analyzed the phosphate profiles. It appears that the varZc parameterization allows more phosphate concentration (Figure 8a,b) in the production zone and thereby increases the corresponding biological production (Figure 8c, d). The net export production in the model during JJAS is consistent with the satellite data (Figure 8d, see also Figure 7a). However, in the constZc case the exports are rather 'flat' throughout the season with imperfect representation of seasonal biological export. The Table 1-4 summarizes all the values discussed here.

The impact of varZc in the biological and solubility pumps is computed as per Louanchi et. al., (1996, see Appendix A). The varZc parameterization has strengthened the biological as well as the solubility pump in the model and thereby modifying the phosphate profiles and achieves a seasonal balance in export versus new production (Figure 9a). During the monsoon period the varZc simulations increases the strength of the solubility pump and biological pump by 10.43 ± 1.3 g C m^{-2} yr^{-1} and 106.52 ± 9 g C m^{-2} yr^{-1} respectively (see Table 5 and 6). Similarly the annual mean strength of solubility pump and biological pump is increased by 3.29 ± 0.6 g C m^{-2} yr^{-1} and 81.18 ± 9.92 g C m^{-2} yr^{-1} respectively. This supports the fact that the varZc parameterization basically modifies the biological pump and solubility pump in the model simulations and thereby improved the seasonal cycle of CO_2 flux and pCO_2.

3.3 Sri Lanka Dome (SLD) ~~Region~~

The seasonal variation in the compensation depth for the SLD has a similar pattern as that of the WAS. The compensation depth deepens to its maximum during March up to 45.23 ± 0.3 m and reaches its minimum during the following monsoon period at 30.79 ± 1.5 m (Figure 5). The similarities of varZc between WAS and SLD indicate that they both are under similar cycles of solar influx and biological production. The SLD chl-a dominates only up to July (Vinayachandran et al., 2004) which explains why production with varZc increases earlier compared to the WAS which occurs during August-October.

The seasonality in CO_2 flux and pCO_2 were compared with Takahashi et al., (2009) observations (Figure 10). The varZc results in a slight improvement in CO_2 flux when compared with constZc (Figure 10a). However, both constZc and varZc simulations underestimate the magnitude of CO_2 flux when compared with observations. The seasonal mean CO_2 flux during the monsoon period is 1.79 mol m^{-2} yr^{-1} from observations, which means SLD region is a source of CO_2. But the mean values of constZc and varZc simulations yield flux values of -0.008 ± 0.2 mol m^{-2} yr^{-1} and 0.24 ± 0.2 mol m^{-2} yr^{-1}, respectively. The constZc simulations misrepresent the SLD region as a sink of CO_2 during monsoon period which is opposite to that of observations. The varZc simulations correct this misrepresentation to a source albeit at a smaller magnitude by 0.24 ± 0.09 mol m^{-2} yr^{-1} for the monsoon period. Compared to observations, the varZc case underestimates the magnitude of JJAS mean by 1.55 mol m^{-2} yr^{-1}.

The annual mean CO_2 fluxes for constZc and varZc simulations are -0.02 ± 0.1 mol m^{-2} yr^{-1} and 0.10 ± 0.2 mol m^{-2} yr^{-1}, respectively. The varZc parameterization leads to an improvement of

471 0.13 ± 0.1 mol m^{-2} yr^{-1} in the annual mean CO_2 flux when compared with constZc simulations.
472 The observational annual mean of CO_2 flux is 0.80 mol m^{-2} yr^{-1} which is highly underestimated
473 by both simulations. This indicates a regulation of biological production of the region by varZc
474 which makes this region a source of CO_2 during monsoon. The role of the solubility pump may
475 also be underestimated due to the biases in the physical drivers and the lack of mesoscale eddy
476 activities in these simulations (Prasanna Kumar et al., 2002; Valsala and Murtugudde, 2015).

477 The seasonality of pCO_2 (Figure 10b) especially in the monsoon period has significantly
478 improved. The mean pCO_2 during the monsoon season from observation over the SLD region is
479 382.44 µatm. The seasonal mean pCO_2 during monsoon period for constZc and varZc
480 simulations are 371.67 ± 6.04 µatm and 379.24 ± 8.9 µatm, respectively. The annual mean pCO_2
481 from observations, constZc and varZc simulations are 380.21 µatm, 370.76 ± 6.1 µatm and
482 374.94 ± 9.6 µatm, respectively. varZc simulations improve the JJAS mean pCO_2 by 7.56 ± 2.8
483 µatm and the annual mean pCO_2 by 4.18 ± 3.5 µatm, which is reflected in CO_2 flux as well. This
484 is likely due to the impact of new biological parameterization in capturing the episodic upwelling
485 in the SLD region which is further investigated by looking at its biological production.

486 The SLD biological production is highly exaggerated by the model for both constZc and
487 varZc simulations (Figure 11a, b). The seasonal mean biological export for the monsoon period
488 is 51.54 g C m^{-2} yr^{-1} as per satellite-derived estimates. However, the constZc and varZc
489 simulations overestimate it at 167.71 ± 59.04 g C m^{-2} yr^{-1} and 151.51 ± 46.4 g C m^{-2} yr^{-1},
490 respectively. This exaggerated export is visible in climatological annual means where for
491 constZc and varZc simulations they are 144.43 ± 49.8 g C m^{-2} yr^{-1} and 156.08 ± 43.8 g C m^{-2} yr^{-1},
492 respectively.

For constZc simulations, new production is overestimated from March to October when compared to observations and the second peak is observed in November (Figure 11a). But the overestimate in new production with varZc is observed only during JJAS period by a value of 26.23 g C m^{-2} yr^{-1}. For the SLD region the varZc parameterization overestimates the export production but minimizes the excess new production, especially in the monsoon period by 64.15 ± 36.4 g C m^{-2} yr^{-1}. This indicates that the varZc parameterization is somewhat successful in capturing the upwelling episode during monsoon over SLD. All values are summarized in Table 1-4.

The solubility and biological pumps are modified by the varZc parameterization significantly when compared with the constZc simulations (Figure 9b). Over the monsoon period the strength of the solubility and biological pumps are improved by 2.81 ± 1.1 g C m^{-2} yr^{-1} and 66.68 ± 9.7 g C m^{-2} yr^{-1}, respectively. Similarly the annual mean strength of solubility and biological pump are increased by 0.99 ± 1.2 g C m^{-2} yr^{-1} and 52.5 ± 5.1 g C m^{-2} yr^{-1} respectively. All the values are provided in Table 5 and 6.

3.4 Sumatra Coast (SC) ~~region~~

The seasonal variation in the compensation depth over the SC region lies between 40 m and 46 m (Figure 5). The seasonal maximum occurs during JFM, especially in March with a depth of 45.5 m. During the monsoon period the compensation depth shoals slightly with a minimum of 41.1 m in July. The variation in Z_c is relatively small as compared to the other regions which is consistent with its relatively low production throughout the year.

514 The seasonality of CO_2 flux and pCO_2 captured by constZc and varZc simulations are shown
515 in Figure 12a, b. The varZc simulations overestimate both CO_2 flux and pCO_2, especially during
516 the monsoon. It is found that the constZc simulations are better compared to varZc simulations.
517 The varZc simulations overestimate the seasonal mean CO_2 flux and pCO_2 by 1.19 mol m^{-2} yr^{-1}
518 and 29.61 µatm, respectively, compared to observations (Table 1). However, constZc produces a
519 better estimate compared with observations for CO_2 flux and pCO_2. The constZc simulations
520 deliver a better annual mean than varZc (Table 1,2). The annual mean bias in constZc and varZc
521 simulations for CO_2 flux is -0.0033 mol m^{-2} yr^{-1} and 0.31 mol m^{-2} yr^{-1}, respectively. Similarly,
522 pCO_2 bias is 1.95 µatm and 9.07 µatm for constZc and varZc simulations.

523 Biological production simulated by the model along SC explains the overestimation of CO_2
524 flux and pCO_2 (Figure 13). Both constZc and varZc simulations greatly overestimate export
525 production in the model. But a small enhancement in the new production during JJAS in constZc
526 case is an indicator of upwelling episodes. The seasonal mean new production during the
527 monsoon from constZc and varZc are 63.64 ± 30.9 g C m^{-2} yr^{-1} and 78.11 ± 29.1 g C m^{-2} yr^{-1},
528 respectively (Table 4). The seasonal mean export production during the monsoon from
529 observations is 58.87 g C m^{-2} yr^{-1} (Table 3). ConstZc simulations represent a better new
530 production, which is seen as a relatively small exaggeration of CO_2 flux and pCO_2. The
531 biological response off SC is found to be better with constZc which is in contradiction to a
532 general improvement found with varZc in the other regions examined here. Such discrepancies
533 over the SC could be due to the effect of Indonesian Throughflow (Bates et al., 2006) which is
534 not completely resolved in the model due to coarse spatial resolution (also see Valsala et al.,
535 2010).

The overestimation of export production by varZc simulations is also evident by the increase in strength of the biological and solubility pumps, respectively (Figure 9c). The annual mean and JJAS mean DIC increases in the production zone due to the biological pump is 67.21 ± 1.3 g C m^{-2} yr^{-1} and 83.62 ± 0.5 g C m^{-2} yr^{-1}, respectively. Similarly the increase in DIC due to the effect of solubility pump during the JJAS period and annual mean are 10.95 ± 5.2 g C m^{-2} yr^{-1} and 3.87 ± 2.2 g C m^{-2} yr^{-1} respectively (see table 5 and 6).

3.5 Seychelles-Chagos Thermocline Ridge (SCTR) ~~region~~

The SCTR is a unique open-ocean upwelling region with a prominent variability in air-sea interactions (Xie et al., 2002). Wind-driven mixing and upwelling of subsurface nutrient rich water play a major role in biological production of this region (Dilmahamod et al., 2016). The seasonal cycle in compensation depth is shown in Figure 5. The maximum compensation depth occurs in November at about 44.94 m and the minimum at 33.2 m in July. The shoaling of compensation depth during the monsoon period shows that the biological parameterization captures the upwelling response over this region.

The seasonality of CO_2 flux and pCO_2 are shown in Figure 14. The Takahashi observations of CO_2 flux shows a peak in June with outgassing of CO_2 during the upwelling episodes. However, both constZc and varZc simulations underestimate this variability. The seasonality of CO_2 flux in varZc shows a significant improvement when compared to constZc simulations, but underestimated when compared to observations. The seasonal mean CO_2 flux during the monsoon for constZc and varZc simulations are 0.82 mol m^{-2} yr^{-1}, -0.32 ± 0.3 mol m^{-2} yr^{-1} and -0.05 ± 0.4 mol m^{-2} yr^{-1}, respectively. This represents a reduction in the seasonal mean sink of

558 CO_2 flux in the SCTR region during the monsoon by 0.27 ± 0.1 mol m^{-2} yr^{-1} bringing it closer to
559 a source region (see Table 1 for details).

560 The improvement brought about in CO_2 flux is supported by the seasonal cycle in pCO_2 .
561 Based on observations, seasonal mean of pCO_2 with constZc during JJAS is underestimated by
562 11.47 µatm, varZc simulations underestimate it by 6.45 µatm. So it is evident that varZc
563 simulations capture the upwelling episodes better, marked by a greater pCO_2 during JJAS period.
564 However, the magnitude of pCO_2 is still underestimated compared to observations (Table 2).

565 Figure 15 shows the biological production of constZc and varZc simulations for SCTR. It is
566 clear that both simulations overestimate the export production and underestimate the new
567 production. The JJAS mean export production from observations, constZc and varZc are 51.08 g
568 C m^{-2} yr^{-1}, 57.39 ± 14.2 g C m^{-2} yr^{-1} and 99.23 ± 29.8 g C m^{-2} yr^{-1}, respectively. The varZc
569 simulations exaggerate the model export production by 48.14 g C m^{-2} yr^{-1}. The varZc simulations
570 improve the JJAS mean new production by 1.14 ± 2.2 g C m^{-2} yr^{-1} (Table 4). The DIC variations
571 due to the biological pump over the monsoon period and the annual mean also support the
572 exaggerated export production. During the monsoon period, the varZc simulations strengthen the
573 biological and solubilitiy pump by 72.64 ± 6.2 g C m^{-2} yr^{-1} and -4.56 ± 1.6 g C m^{-2} yr^{-1},
574 respectively when compared to the constZc simulations (Figure 9d). This is also reflected in the
575 annual mean DIC variations due to the biological and solubility pump effects (see table 5 and 6).
576 This slight improvement in the model new production, especially during the monsoon period
577 signals that the spatially and temporally varying compensation depth better captures the
578 upwelling over SCTR. Considering the annual mean values of model export and new production,
579 constZc simulations are reasonably faithful to observations.

The underestimation of CO_2 and pCO_2 as well as the exaggeration of model export production and a slight overestimate in model new production may be due to two reasons. (1) SCTR is a strongly coupled region with remote forcing of the mixed layer – thermocline interactions (Zhou et al., 2008) which can affect the seasonality in biological production that the model may not be resolving reasonably, (2) the bias associated with physical drivers, especially wind stress may underestimate the CO_2 flux as well biological production. A similar overestimation of biological production was also reported in a coupled biophysical model (Dilmahamod et al., 2016).

Table 1 – 4 shows the entire summary of seasonal and annual mean CO_2 flux, pCO_2 and biological production reported in Section 3.

4. Sensitivity Simulations

From the analysis of four major upwelling regions over Indian Ocean, it is evident that the biological parameterization of spatio-temporally varying compensation depth better captures upwelling episodes and thus it enhances the model export production. This is most clearly visible over the WAS. In order to quantify how much the varZc parameterization contributed to seasonality of carbon cycle, two additional sensitivity simulations were carried out; (1) with annual mean offline currents and (2) annual mean offline temperatures with the ~~notion~~goal of suppressing the dynamical and thermodynamical effects of seasonal upwelling over the WAS (see Section 2 for details). The focus on this region is motivated by its prominence as the most productive zone of the Indian Ocean. Moreover, the improvement in the biological processes in

the model by the varZc parameterization is best captured in this region. The results are discussed ~~in detail in the following subsections~~ below.

4.1 Impact of varZc parameterization on ~~in~~ seasonality of carbon cycle with annual mean currents.

To quantify the impact of varZc parameterization, the model is forced with annual mean currents only over the WAS with unaltered currents in the rest of the ocean. The hypothesis is that the muting of the seasonal variability of Ekman divergence removes the upwelling and the biological pump contribution to production and carbon cycle. The comparison of constZc and varZc then allows us to decipher the impact of varZc on capturing the impacts of upwelling on biological production and the carbon cycle. The smooth blending of currents at the boundary of the WAS domain is achieved by a linear smoothing function as given in Section 2.

The model biological responses (inferred by comparing with the control run) in terms of the CO_2 flux shows a flat pattern over the monsoon period for constZc simulations [Figure ~~15~~16(a)]. While the varZc simulation~~s~~ forced with the annual mean currents shows an enhanced CO_2 flux indicating the outgassing of CO_2 flux in the WAS due to wind-driven upwelling (Figure ~~15~~16(b)). This qualitatively shows that the spatially and temporally varying compensation depth itself has improved the seasonality in the biological processes (export and new production) and captured the upwelling episodes during the monsoon. The varZc parameterization is responsible for improvement of 0.48 ± 0.04 mol m^{-2} yr^{-1} and 0.13 ± 0.02 mol m^{-2} yr^{-1} ~~during~~ in the JJAS seasonal and annual mean CO_2 flux~~es~~, respectively. This improves the overall model CO_2 flux in the control run especially in July (Figure ~~15~~16(b)).

Similar improvements were also noticed in pCO_2 (Figure ~~16~~17). In the constZc simulations with annual mean currents, the pCO_2 dips down during JJAS monsoon period which indicates the inadequacy of constZc in capturing the upwelling enriched pCO_2 difference (Figure ~~16~~17a, b). The varZc simulation slightly modifies the pCO_2 in the 'right' direction during JJAS despite the annual mean currents.

The export ~~production~~ and ~~the~~ new productions in the model explain the modification of CO_2 flux and pCO_2 by varZc parameterization. The biological export production is highly underestimated in the constZc simulations forced with annual mean currents while the varZc simulations captures the seasonal upswing in production (Figure ~~17~~18). The improved JJAS mean and annual mean export production by 43.51 ± 8.6 g C m^{-2} yr^{-1} and 30.28 ± 13.7 g C m^{-2} yr^{-1}, respectively is a clear indication of the positive impacts of a variable Zc. Similarly the improvement in JJAS mean and annual mean new production (Figure ~~18~~19) from varZc simulated with annual mean currents ~~were~~ are 17.39 ± 0.8 g C m^{-2} yr^{-1} and 14.81 ± 0.1 g C m^{-2} yr^{-1}, respectively. In short the varZc biological parameterization improves the export and new productions in the model. This helps the model to capture the upwelling episodes over the study regions. Table ~~5~~7 summarizes all the results of biological sensitivity runs.

4.2 Impact of varZc parameterization on ~~in~~ seasonality of carbon cyle with annual mean temperatures.

Using the annual mean temperature over the WAS, we are suppressing the cooling effect of temperature due to upwelling and quantifying how much the model seasonality is improved ~~by means of~~ due to varZc parameterization. (see Section 2 for details). The varZc simulations

forced with annual mean SST has ~~greater~~ larger JJAS mean and annual mean CO_2 fluxes by 0.88 ± 0.1 mol m^{-2} yr^{-1} and 0.28 ± 0.07 mol m^{-2} yr^{-1}, respectively (Figure ~~19~~20 and Table ~~6~~8). For a given annual mean SST the solubility pump largely controls the CO_2 emission during JJAS if a variable Zc is prescribed, likely by the enrichment ~~in the~~ of DIC (inferred from Figure 8b). Similarly the improvement in pCO_2 (Figure ~~20~~21) with varZc simulation is also remarkable. The JJAS mean and annual mean improvements from the implementation of varZc are 11.05 ± 1.9 µatm and 1.91 ± 1.4 µatm, respectively. The detailed quantification of CO_2 and pCO_2 responses for this experimental setup is given in Table ~~6~~8. The above analysis adds supporting evidence that the varZc simulations strengthen the seasonality of the model compared to the constZc case. This is presumably accomplished by the more accurate compensation depth and production zone implied with a variable Zc.

5. Summary and Conclusions

A spatially and temporally varying compensation depth parameterization as a function of solar radiation and Chl-a is implemented in the biological pump model of OCMIP-II for a detailed analysis of biological fluxes in the upwelling zones of the Indian Ocean. The varZc parameterization improves the seasonality of model CO_2 flux and pCO_2 variability, especially during the monsoon period. A s~~S~~ignificant improvement is observed in ~~the~~ WAS where the monsoon wind-driven upwelling dominates biological production. The magnitude of CO_2 flux matches with observations, especially in July when monsoon winds are at their peak. Monsoon triggers upwelling in SLD as well which acts as a source of CO_2 to the atmosphere. The seasonal

667 and annual mean are underestimated with constZc and the SLD is reduced to a sink of CO_2 flux.
668 The varZc simulations modify the seasonal and annual means of CO_2 flux of SLD and depict it
669 as a source of CO_2 especially during the monsoon, but the magnitude is still underestimated
670 compared to Takahashi et al., (2009) observations. The SCTR variability is underestimated by
671 both constZc and varZc simulations, portraying it as a CO_2 sink region whereas observations
672 over the monsoon period indicate that the thermocline ridge driven by the open ocean wind-
673 stress curl is in fact an oceanic source of CO_2. However, the varZc simulation reduces~~d~~ the
674 magnitude of the sink in this region bringing it relatively closer to observations.

675 VarZc biological parameterization strengthens the export and new productions in the model,
676 which allows it to a represent a better seasonal cycle of CO_2 flux and pCO_2 over the study
677 regions. The WAS export production is remarkably improved by 62.37 ± 7.8 g C m^{-2} yr^{-1}
678 compared to constZc. This supports our conclusion that the varZc parameterization increases the
679 strength of biological export in the model. Over the SLD, the JJAS seasonal mean export and
680 new productions are underestimated in varZc compared to constZc simulations, but the annual
681 mean export production is improved. Export production at ~~the~~ SC and SCTR are highly
682 exaggerated and there is hardly any improvement in new production with a variable Zc
683 especially over the monsoon period. The inability of varZc parameterization to improve the
684 seasonality of SC and SCTR may be due to the interannnual variability of biological production
685 associated with the Indonesian throughflow and remote forcing of the mixed layer-thermocline
686 interactions and the effect of biases in the windstress data used as a physical driver in the model.

687 ~~Further s~~Sensitivity experiments carried out ~~with providing~~ by prescribing annual mean
688 currents or temperatures ~~in~~ over selected subdomains reveal that the varZc retains the seasonality
689 of carbon fluxes, pCO_2, and export and new productions ~~in the right direction as in the~~ closer to

observations. This strongly supports our contention that varZc parameterization improves ~~the~~ export and new productions and it is also efficient in capturing upwelling episodes of the study regions. This points out the significant role of having a ~~proper~~ close balance in seasonal biological export and new production in models to capture the seasonality in carbon cycle. This also confirms the role of biological and solubility pumps in producing the seasonality of carbon cycle in the upwelling zones.

However the underestimation of seasonality of CO_2 flux over the SLD and overestimation over the SC as well as the SCTR ~~is~~are a cautionary flag for the study. This uncertainty poses an important scientific question as to whether the model biology over the SC and SCTR region is not resolving the seasonality in CO_2 flux and pCO_2 properly or whether the seasonality in the compensation depth is not able to fully capture the biological processes.

To address these questions we have used an inverse modeling ~~methods~~ approach (Bayesian inversion) in order to optimize the spatially and temporally varying compensation depth using surface pCO_2 as the observational constraints and computed the optimized biological production. The results will be reported elsewhere.

Appendix - A

For $Z < Z_c$,

$$J_{prod} = \frac{1}{\tau}([PO_4] - [PO_4^*]), \qquad [PO_4] > [PO_4^*] \tag{A1}$$

$$J_{DOP} = \sigma J_{prod} - \kappa[DOP] \tag{A2}$$

$$J_{PO4} = -J_{prod} + \kappa[DOP] \tag{A3}$$

$$J_{ca} = Rr_{C:P}(1-\sigma)J_{prod} \tag{A4}$$

$$J_{DIC} = r_{C:P}J_{PO4} + J_{ca} \tag{A5}$$

$$J_{ALK} = -r_{N:P}J_{PO4} + 2J_{ca} \tag{A6}$$

For $Z > Z_c$,

$$J_{prod} = 0, \qquad [PO_4] \leq [PO_4^*] \tag{A7}$$

$$J_{DOP} = -\kappa[DOP] \tag{A8}$$

$$J_{PO4} = -\frac{\partial F}{\partial Z} + \kappa[DOP] \tag{A9}$$

$$F(Z) = F_c\left(\frac{Z}{Zc}\right)^{-a} \tag{A10}$$

$$F_c = (1-\sigma)\int_0^{Zc} J_{prod}\, dZ \tag{A11}$$

$$J_{ca} = -\frac{\partial F_{Ca}}{\partial Z} \tag{A12}$$

$$F_{Ca} = Rr_{C:P}F_C e^{-(z-Zc)/d} \tag{A13}$$

Where Z is the depth and Z_c is the compensation depth in the model. J_{prod} , J_{DOP} ,J_{PO4}, J_{Ca} are the biogeochemical sources and sinks. Within the compensation depth (Z_c), the biological production in the model J_{prod} is calculated using equation A1. $[PO_4]$ is the model phosphate concentration and $[PO_4^*]$ is observational phosphate. τ is the restoration timescale taken as 30 days. Whenever the model phosphate exceeds the observational phosphate, it allows production.The observational phosphate data were taken from the World Ocean Atlas (WOA; Garcia et al., 2014). ~~(WOA) 1994 [Conkright et al., 1994]~~. During the biological production a fixed fraction (σJ_{prod}) of phosphate is converted into Dissolved Organic Phosphate (DOP) which is a source for J_{DOP} [equation A2] and remaining– $\kappa[DOP]$is exported downward below the compensation depth, which is further remineralized into inorganic phosphate and made available for further biological production [equation A3]. The downward flux of phosphate which is not converted into DOP within the compensation depth is given by equation A11. The decrease of flux with depth due to remineralization is shown by equation A10. The values of the constants a, κ, σ are 0.9, $(0.2 \text{ year})^{-1}$ to $(0.7 \text{ year})^{-1}$, 0.67, respectively. The rate of production is used to explain the formation of calcium carbonate cycle in the surface waters [equation A4] and its export is given by equation A12. Where R is the rain ratio, a constant molar ratio of exported particulate organic carbon to the exported calcium carbonate flux at compensation depth. The exponential decrease of calcium carbonate flux with scale depth d is given by equation A13. The biological source or biological sink of dissolved inorganic carbon (DIC) and alkalinity (ALK) is explained through equations A5 and A6, respectively. Where the values of rain ratio (R) is taken as 0.07 and the Redfield ratio, $r_{C:P} = 106$,$r_{N:P} = 16$ and scale depth d is chosen as 3500m.

Biological and Solubility Pump calculation

The biological effect on DIC is calculated from Louanchi et al., (1996). The tendency of DIC due to biomass production and calcite formation in the production zone is expressed as below.

$$\left(\frac{\partial DIC}{\partial t}\right)_b = \left(\frac{\partial PO_4}{\partial t}\right)_b \times R_{C:P} - J_{Ca} \qquad \text{(A14)}$$

The total tendency of DIC in the production zone is:

$$\left(\frac{\partial DIC}{\partial t}\right)_{total} = \left(\frac{\partial DIC}{\partial t}\right)_b + \int_x \int_y \Phi dx\, dy \qquad \text{(A15)}$$

where $\left(\frac{\partial DIC}{\partial t}\right)_b$ is the evolution of DIC due to the impact of biology (i.e. biological pump). The first term in the R.H.S of Equation A14 is the rate of change of phosphate which represents the biological production in the model multiplied by the phosphorous to carbon Redfield ratio ($R_{C:P}$ = 117:1) and J_{Ca} represents the calcite formation in the model (see Equation A12). The solubility pump is calculated as the surface integral of the flux Φ (Louanchi et. al., 1996).

Acknowledgement

The OCMIP-II routines were taken from (http://ocmip5.ipsl.jussieu.fr/OCMIP/). GFDL data for OTTM is taken from (http://data1.gfdl.noaa.gov/nomads/forms/assimilation.html).Takahashi data is taken from (http://www.ldeo.columbia.edu/res/pi/CO2/).The computations were carried out in High Performance Computing (HPC) of Ministry of Earth Sciences (MoES), IITM. Ms. Shikha Singh, Ms. Anju M (IITM) and Mr. Saran Rajendran (CUSAT) are thanked for initial helps and discussions.

References

Anderson, L. A., Sarminento. J. L.: Global ocean phosphate and oxygen simulations, Global Biogeochem. Cycles., 9, 621-636, doi:10.1029/95GB01902, 1995.

Asselin, R.: Frequency filter for time integrations, Mon. Wea. Rev., 100, 487–490, doi: 10.1175/1520-0493, 1972.

Banse, K., McClain, C. R.: Winter blooms of phytoplankton in the Arabian Sea as observed by the Coastal Zone Color Scanner, Mar. Ecol. Prog. Ser., 34, 201 – 211, 1986.

Banse, K.: Seasonality of phytoplankton chlorophyll in the central and northern Arabian Sea, Deep Sea Res., 34, 713 – 723, doi:10.1016/0198-0149, 1987.

Barber, R. T., Marra. J., Bidigare. R. C., Codispoti. L. A., Halpern. D., Johnson. Z., Latasa. M., Goericke. R., and Smith. S. L.: Primary productivity and its regulation in the Arabian Sea during 1995, Deep. Sea. Res, pt. II, 48, 1127 – 1172. doi:10.1016/S0967-0645, 2001.

Bates, N. R., Pequignet. A. C., and Sabine. C. L.: Ocean carbon cycling in the Indian Ocean: 2. Estimates of net community production, Global Biogeochem. Cycles., 20, GB3021, doi:10.1029/2005GB002492, 2006.

Bauer, S., Hitchcock, G. L., Olson, D. B.: Influence of monsoonally-forced Ekman dynamics upon surface-layer depth and plankton biomass distribution in the Arabian Sea, Deep Sea Res., 38, 531 – 553, doi:10.1016/0198-0149, 1991.

Behrenfeld, M. J., Falkowski. P. G.: Photosynthetic rates derived from satellite-based chlorophyll concentration, Limnol. Oceanogr., 42, 1 – 20, doi: 10.4319/lo.1997.42.1.0001, 1997.

Boyd, P. W., Rynearson, T. A., Armstrong, E. A., Fu. F., Hayashi. K. and co-authors.: Marine Phytoplankton Temperature versus growth responses from polar to tropical waters – outcome of a scientific community-wide study, PLoS ONE 8(5)., e63091, Doi:10.1371/journal.phone.0063091, 2013.

Brock, J C., McClain, C. R.: Interannual variability of the southwest monsoon phytoplankton bloom in the north-western Arabian Sea, J. geophys. Res., 97(C1), 733 – 750, doi/10.1029/91JC02225, 1992.

Brock, J. C., McClain, C. R., Hay, W. W.: A southwest monsoon hydrographic climatology for the northwestern Arabian Sea, J. geophys. Res., 97(C6), 9455 – 9465, doi: 10.1029/92JC00813, 1992.

Brock, J. C., McClain, C. R., Luther, M. E., Hay, W. W.: The phytoplankton bloom in the northwestern Arabian Sea during the southwest monsoon of 1979, J. geophys. Res., 96(C11), 623 – 642, doi: 10.1029/91JC01711, 1991.

Brock. J., Sathyendranath. S., and Platt. T.: Modelling the seasonality of subsurface light and primary production in the Arabian Sea, Mar. Eco. Prog. Ser., 101, 209 – 221, 1993.

Bruce, J. G.: Some details of upwelling off the Somali and Arabian coasts, J. mar. Res., 32, 419 – 423, 1974.

Bryan. K., Lewis, L. J.: A water mass model of the world ocean, J. Geophys. Res., 84, 2503 – 2517, doi: 10.1029/JC084iC05p02503, 1979.

825 Chang, Y. S., Zhang. S., Rosati. A., Delworth. T., Stern. W. F.: An assessment of oceanic
826 variability for 1960-2010 from the GFDL ensemble coupled data assimilation, Clim. Dyn., 40,
827 775 – 803, doi: 10.1007/s00382-012-1412-2, 2012.

828 Christian J. R., Verschall M. A., Murtugudde R., Busalacchi A. J., McClain C. R.:
829 Biogeochemical modelling of the tropical Pacific Ocean. II: Iron biogeochemistry, Deep Sea
830 Res., 49, 545 – 565, doi:10.1016/S0967-0645, 2001.

831 Colwell, R. R.: Global climate and infectious disease: the cholera paradigm, Science., 274(5295),
832 2025 – 2031, doi: 10.1126/science.274.5295.2025, 1996.

833 Dilmahamod A. F., Hermes. J. C., Reason C. J. C.: Chlorophyll-a variability in the Seychelles-
834 Chagos Thermocline Ridge: Analysis of a coupled biophysical model, J. of. Mar. Sys., 154, 220
835 – 232, doi:10.1016/j.jmarsys.2015.10.011, 2016.

836 Doney S. C., and co-authors.: Evaluating global ocean carbon models: The importance of
837 realistic physics, Glob. Biogeochem. Cycles., 18, doi:10.1029/2003GB002150, 2004.

838 Eppley, R. W., Peterson. B. J.: Particulate organic matter flux and planktonic new production in
839 the deep ocean, Nature., 282, 677-680, doi:10.1038/282677a0, 1979.

840 Eppley, R. W.: Temperature and phytoplankton growth in the sea, Fish. Bull., 70, 1063 – 1085,
841 1972.

842 Feely, R. A., Sabine, C. L., Takahashi, T., Wanninkhof, R.: Uptake and Storage of Carbon
843 Dioxide in the Ocean: The Global CO_2 Survey, Oceanography., 14(4), 18–32,
844 doi:10.5670/oceanog.2001.03, 2001.

Friedrichs, M. A. M., and co-authors.: Assessment of skill and portability in regional biogeochemical models: role of multiple planktonic groups, J. GeoPhy. Res., 112, doi: 10.1029/2006JC003852, 2007.

Friedrichs, M. A. M., Hood, R. R., Wiggert, J. D.: Ecosystem complexity versus physical forcing quantification of their relative impact with assimilated Arabian Sea data, Deep Sea Res., 53, 576-600, doi:10.1016/j.dsr2.2006.01.026, 2006.

Garcia, H. E., R. A. Locarnini, T. P. Boyer, J. I. Antonov, O.K. Baranova, M.M. Zweng, J.R. Reagan, D.R. Johnson.: World Ocean Atlas 2013, Volume 4: Dissolved Inorganic Nutrients (phosphate, nitrate, silicate), S. Levitus, Ed., A. Mishonov Technical Ed.; NOAA Atlas NESDIS 76, 25 pp, 2014.

Garcia, H. E., R. A. Locarnini, T. P. Boyer, J. I. Antonov, O.K. Baranova, M.M. Zweng, J.R. Reagan, D.R. Johnson.: World Ocean Atlas 2013, Volume 4: Dissolved Inorganic Nutrients (phosphate, nitrate, silicate), S. Levitus, Ed., A. Mishonov Technical Ed.; NOAA Atlas NESDIS 76, 25 pp, 2014.

Gattuso, J. P., B. Gentili, C. M. Duarte, J. A. Kleypas, J. J. Middelburg, and D. Antoine.: Light availability in the coastal ocean: Impact on the distribution of benthic photosynthetic organisms and their contribution to primary production, Biogeosciences, 3, 489 – 513, doi:10.5194/bg-3-489-2006, 2006.

Gent, P. R., McWilliams. J. C.: Isopycnal mixing in ocean circulation models, J. Phys. Oceanogr., 20, 150 – 155, doi: 10.1175/15200485, 1990.

865 Harwell, C., Kim, K., Burkholder, J., Colwell, R., Epstein, P. R., Grimes, D., Hofmann, E. E.,
866 Lipp, E. K., Osterhaus, A., and Overshreet, R. M.: Emerging marine diseases-climate links and
867 anthropogenic factors, Science., 285(5433), 1505 – 1510, doi: 10.1126/science.285.5433.1505,
868 1999.

869 Howden, S., Murtugudde, R.: Effects of river inputs into the Bay of Bengal, J. Geophys. Res.,
870 106, 19,825-19,843. doi: 10.1029/2000JC000656, 2001.

871 Jerlov N. G.: Marine optics, Second ed., Elsevier, pp 231, 1976.

872 Jung, E., and Kirtman. B. P.: ENSO modulation of tropical Indian ocean subseasonal variability,
873 Geophy. Res. Lett., 43, doi: 10.1002/2016GL071899, 2016.

874 Krey, J., Bahenerd, B.: Phytoplankton production atlas of the international Indian Ocean
875 expedition, Institut fur Meereskundeander Universitat Kiel, Kiel, German.

876 Large, W. G., McWilliams, J. C., Doney, S. C.: Oceanic vertical mixing: A review and a model
877 with a nonlocal boundary layer parameterization, Rev. Geophys., 32, 363 – 403, doi:
878 10.1029/94RG01872, 1994.

879 Le Quere, C., Orr, J. C., Monfray, P., Aumont, O.: Interannual variability of the oceanic sink of
880 CO_2 from 1979 through 1997, Global Biogeochem. Cycles., 14, p1247 – 1265, doi:
881 10.1029/1999GB900049, 2000.

882 Lee, P. F., Chen, I. C., Tzeng. W. N.: Spatial and Temporal distributions patterns of bigeye tuna
883 (Thunnusobsesus) in the Indian Ocean, Zoological studies-Taipei-, 44(2), 260, 2005.

884 Lehodey .P., Senina I., Sibert. J., Bopp. L., Calmettes B., Hampton .J., Murtugudde. R.:
885 Preliminary forecasts of Pacific bigeye tuna population trends under the A2 IPCC scenario, Prog
886 in Oceanography., 86, 302 – 315, doi:10.1016/j.pocean.2010.04.021, 2010.

887 Levy, M., Shankar, D., Andre, J. M., Shenoi, S., Durand, F., Montegut, C. B., 2007. Basin-wide
888 seasonal evolution of the Indian Ocean's phytoplankton blooms, J. Geophy. Res. Oceans.,
889 112(C12), 1978 – 2012, doi: 10.1029/2007JC004090, 2007.

890 Liao, X., Zhan, H., Du, Y.: Potential new production in two upwelling regions of the Western
891 Arabian Sea: Estimation and comparison, J. Geophy. Res. Oceans., 121,
892 doi:10.1002/2016JC011707, 2016.

893 Lopez-Urrutia, A., E. San Martin, R. P. Harris, and X. Irigoien.: Scaling the metabolic balance of
894 the oceans, Proc. Natl. Acad. Sci. U.S.A., 103, 8739-8744,doi:10.1073/pnas.0601137103, 2006.

895 Marra, J. F., Veronica P. Lance, Robert D. Vaillancourt, Bruce R. Hargreaves.: Resolving the
896 ocean's euphotic zone, Deep Sea. Res. pt. I., 83, 45 -50, doi:10.1016/j.dsr.2013.09.005, 2014.

897 Matsumoto K., Tokos. K. S., Price., A. R., Cox. S. J.: First description of the Minnesota Earth
898 System Model for Ocean biogeochemistry (MESMO 1.0), Geosci. Model Dev., 1, 1-15,
899 doi:10.5194/gmd-1-1-2008, 2008.

900 McCreary, J., Murtugude, R., Vialard, J., Vinayachandran, P., Wiggert, J. D., Hood, R. R.,
901 Shankar, D., Shetye, S.: Biophysical processes in the Indian Ocean, Indian Ocean
902 Biogeochemical Processes and Ecological Variability., 9 – 32, doi: 10.1029/GM185, 2009.

903 Moisan, J. R., Moisan, A. T., Abbott, M. R.: Modelling the effect of temperature on the
904 maximum growth rates of phytoplankton populations, Eco. Modelling., 153, 197-215,
905 doi:10.1016/S0304-3800(02)00008, 2002.

906 Morel, A.: Optical modeling of the upper ocean in relation to its biogenous matter content (Case
907 1 Waters), J. Geophys. Res., 93, 10479-10, 768, doi: 10.1029/JC093iC09p10749, 1988.

908 Murtugudde R., McCreary J. P., Busalacchi, A. J.: Oceanic processes associated with anomalous
909 events in the Indian Ocean with relevance to 1997-1998, J. Geophy. Res., 105, 3295-3306, doi:
910 10.1029/1999JC900294, 2000.

911 Murtugudde, R., Busalacchi, A. J.: Interannual variability of the dynamics and thermodynamics
912 of the tropical Indian Ocean, J. Clim. 12, 2300-2326, doi:10.1175/1520-0442, 1999.

913 Murtugudde, R., Seager, R., Thoppil, P.: Arabian Sea response to monsoon variations,
914 Paleoceanography., 22, PA4217, doi:10.1029/2007PA001467, 2007.

915 Najjar, R. G., Keeling, R. F.: Analysis of the mean annual cycle of the dissolved oxygen
916 anomaly in the world ocean, J. Mar. Res., 55, 117 – 151, doi:10.1357/0022240973224481, 1997.

917 Najjar, R. G., Orr, J. C.: Design of OCMIP-2 simulations of chlorofluorocarbons, the solubility
918 pump and common biogeochemistry, http://www.ipsl.jussieu.fr/OCMIP/., 1998.

919 Najjar, R. G., Sarmiento, J. L., Toggweiler, J. R.: Downward transport and fate of organic matter
920 in the ocean: simulations with a general circulation model, Global biogeochem. Cycles., 6, 45-
921 76, doi/10.1029/91GB02718, 1992.

922 Naqvi, S. W. A., Moffett, J. W., Gauns, M. U., Narvekar, P. V., Pratihary, A. K., Naik, H.,
923 Shenoy, D. M., Jayakumar, D. A., Goepfert, T. J., Patra, P. K., Al-Azri, A., and Ahmed, S. I.:

924 The Arabian Sea as a high-nutrient, low-chlorophyll region during the late Southwest Monsoon,
925 Biogeosciences., 7, 2091-2100, doi:10.5194/bg-7-2091-2010, 2010.

926 Naqvi, S., Naik, H., Narvekar, P.: The Arabian Sea, in Biogeochemistry, edited by K. Black and
927 G. Shimmield, pp. 156 – 206, Blackwell, Oxford, 2003.

928 Orr, J. C. and co-authors.: Estimates of anthropogenic carbon uptake from four three-
929 dimensional global ocean models, Glob. Biogeochem. Cycles., 15, p43 – 60, doi:
930 10.1029/2000GB001273, 2001.

931 Orr, J. C., Aumont, O., Bopp, L., Calderia, K., Taylor, K., et. al.: Evaluation of seasonal air-sea
932 CO2 fluxes in the global carbon cycle models, International open Science conference (Paris, 7-
933 10 Jan. 2003), 2003.

934 Osawa, T., Julimantoro, S.: Study of fishery ground around Indonesia archipelago using remote
935 sensing data, International archives of the Photogrammetry, Remote sensing and spatial
936 information science., vol XXXVIII, part-8, 2010.

937 Parsons, T. R., Takahashi, M., Habgrave, B.: In Biological Oceanographic Processes, 3rd ed.,
938 330pp., Pergamon Press, New York, doi: 10.1002/iroh.19890740411, 1984.

939 Prasanna Kumar, .S., Muraleedharan, P. M., Prasad, T. G., Gauns, M., Ramaiah, N., de Souza, S.
940 N., Sardesai, S., Madhupratap, M.: Why is the Bay of Bengal less productive during summer
941 monsoon compared to the Arabian Sea?, Geophys. Res. Lett., 29(24), 2235,
942 doi:10.1029/2002GL016013, 2002.

943 Prasanna Kumar, S., Roshin, P. R., Narvekar, J., Dinesh Kumar, P., Vivekanandan, E.: What
944 drives the increased phytoplankton biomass in the Arabian Sea?, Current Science, 99(I), 101 –
945 106, 2010.

946 Prassana Kumar. S, Ramaiah. N, Gauns. M., Sarma V. V. S. S., Muraleedharan. P. M.,
947 RaghuKumar. S., Dileep Kumar., Madhupratap. M.: Physical forcing of biological productivity
948 in the Northern Arabian Sea during the Northeast Monsoon, Deep Sea Res. Pt. II., 48, 1115-
949 1126, doi:10.1016/S0967-0645(00)00133-8, 2001.

950 Praveen, V., Ajayamohan**,** R. S., **Valsala,** V., Sandeep, S.: Intensification of upwelling along
951 Oman coast in a warming scenario, Geophys. Res. Lett., 43, doi:10.1002/2016GL069638, 2016.

952 Qasim, S. Z.: Biological productivity of the Indian Ocean, J. mar. Sci., 6, 122 – 137, 1977.

953 Qasim, S. Z.: Oceanography of Northern Arabian Sea, Deep Sea Res., 29(9A), 1041 – 1068,
954 doi:10.1016/0198-0149(82)90027-9, 1982.

955 Redi, M.: Oceanic isopycnal mixing by coordinate rotation, J. Phys. Oceanogr., 12, 1154 – 1158,
956 doi: 10.1175/1520-0485, 1982.

957 Regaudie-de-Gioux, A., and C. M. Duarte.: Compensation irradiance for planktonic community
958 metabolism in the ocean, Global Biogeochem. Cycles, 24, GB4013,
959 doi:10.1029/2009GB003639, 2010.

960 Roxy, M. K., Modi, A., Murtugudde, R., Valsala, V., Panickal, S., Prasanna Kumar, S.,
961 Ravichandran, M., Vichi, M., Levy, M.: A reduction in marine primary productivity driven by
962 rapid warming over the tropical Indian Ocean, 43, 826 – 833, J. Geophy. Res. Letters.,
963 doi:10.1002/2015GL066979, 2015.

964 Ryther, J., Menzel, D.: On the production, composition, and distribution of organic matter in the
965 Western Arabian Sea, Deep Sea Research and Oceanographic Abstracts., 12(2), 199 -209.
966 doi:10.1016/0011-7471(65)90025-2, 1965.

967 Ryther, J.: Photosynthesis in the ocean as function of light Intensity, Limnol. Oceanogr., vol 1,
968 issue 1, doi: 10.4319/lo.1956.1.1.0061, 1956.

969 Sarma V. V. S. S.: Net plankton community production in the Arabian Sea based on O_2 mass
970 balance model, Glob. biogeochem. Cycles., 18, GB4001, doi:10.1029/2003GB002198, 2004.

971 Sarma, V. V. S. S.: An evaluation of physical and biogeochemical processes regulating the
972 perennial suboxic conditions in the water column of the Arabian Sea, Global Biogeochem.
973 Cycles., 16, doi:10.1029/2001GB001461, 2002.

974 Sarmiento, J. L., and Gruber, N.: Ocean Biogeochemical Dynamics, Princeton University Press,
975 New Jersey, 2006.

976 Sarmiento, J. L., Monfray. P., Maier-Reimer., Aumont, O., Murnane, R. J., Orr, J. C.: Sea-air
977 CO_2 fluxes and carbon transport: A comparison of three ocean general circulation models,
978 Global Biogeochem. Cycles., 14, p1267 – 1281. doi: 10.1029/1999GB900062, 2000.

979 Schott, F.: Monsoon response of the Somali current and associated upwelling, Prog.Oceanogr.,
980 12, 357 – 381, doi:10.1016/0079-6611(83)90014-9, 1983.

981 Smetacek, V., and Passow, U.: Spring bloom initiation and Sverdrup's critical depth model,
982 Limnol. Oceanogr., 35, 228 – 234, doi: 10.4319/lo.1990.35.1.0228, 1990.

983 Smith, L. S.: Understanding the Arabian Sea: Reflections on the 1994-1996 Arabian Sea
984 Expedition, Deep Sea Res. Pt. II., 48, 1385-1402, doi:10.1016/S0967-0645(00)00144-2, 2001.

985 Smith, R. L., Bottero, L. S.: On upwelling in the Arabian Sea. In Angel, M (ed) A voyage of
986 Discovery. Pergammon Press, New York, p. 291 – 304, 1977.

987 Smith, S. L., Codistpoti, L. A.: Southwest monsoon of 1979: chemical and biological response of
988 Somali coastal waters. Science, 209, 597 – 600. doi:10.1126/science.209.4456.597, 1980.

989 Smith, S. L.: Biological indications of active upwelling in the northwestern Indian Ocean in 1964
990 and 1979, a comparison with peru and northwest Africa, Deep Sea Res., 31, 951 – 967,
991 doi:10.1016/0198-0149(84)90050-5, 1984.

992 Susanto. R., Gordon, A. L., Zheng. Q.: Upwelling along the coasts of Java and Sumatra and its
993 relation to ENSO, J. Geophy. Res. Lett., 28, 1599-1602, doi: 10.1029/2000GL011844, 2001.

994 Swallow, J. C.: Some aspects of the physical oceanography of the Indian Ocean, Deep Sea Res.,
995 31, 639 – 650, doi:10.1016/0198-0149(84)90032-3, 1984.

996 Takahashi, T., Sutherland, S. C., Wanninkhof, R., Sweeney, C., Feely, R. A., Chipman, D. W.,
997 Hales, B., Friederich, G., Chavez, F., Sabine, C., et al.: Climatological mean and decadal
998 changes in surface ocean pCO_2 and net sea-air CO_2 flux over the global oceans. Deep Sea Res.,
999 Pt. II., 56, 554 – 557, doi:10.1016/j.dsr2.2008.12.009, 2009.

1000 Valsala, V.: Different spreading of Somali and Arabian coastal upwelled waters in the northern
1001 Indian Ocean: A case study. J. Phy. Oceanogr., 803 – 816, doi: https://doi.org/10.1007/s10872-
1002 009-0067-z, 2009.

1003 Valsala V., Maksyutov, S.: A short surface pathway of the subsurface Indonesian Throughflow
1004 water from the Java Coast associated with upwelling, Ekman Transport, and Subduction. Int. J.
1005 Oceanogr., 15, doi: 10.1155/2010/540743, 2010.

Valsala V., Maksyutov, S.: Interannual variability of air-sea CO_2 flux in the north Indian Ocean, Ocean Dynamics., 1 – 14, doi 10.1007/s10236-012-0588-7, 2013.

Valsala, K. V., Maksyutov, S., Ikeda, M.: Design and Validation of an offline oceanic tracer transport model for a carbon cycle study, J. clim., 21, doi: 10.1175/2007JCLI2018.1, 2008.

Valsala, V., Maksyutov, S., Murtugudde, R.: Interannual to Interdecadal Variabilities of the Indonesian Throughflow Source Water Pathways in the Pacific Ocean, J. Phys. Oceanogr., 41, 1921–1940, doi: 10.1175/2011JPO4561.1, 2011.

Valsala, V., Maksyutov, S.: Simulation and assimilation of global **oc**ean pCO_2 and air-sea CO_2 fluxes using ship observations of surface ocean pCO_2 in a simplified biogeochemical model, Tellus., 62B, doi: 10.1111/j.1600-0889.2010.00495, 2010.

Valsala, V., Murtugudde, R.: Mesoscale and Intraseasonal Air-Sea CO_2 Exchanges in the Western Arabian Sea during Boreal Summer, Deep Sea Res. Pt. I, 103, 103-113, doi:10.1016/j.dsr.2015.06.001, 2015.

Valsala, V., Roxy, M., Ashok, K., Murtugudde, R.: Spatio-temporal characteristics of seasonal to multidecadal variability of pCO_2 and air-sea CO_2 fluxes in the equatorial Pacific Ocean, J. Geophys. Res., 119, 8987 – 9012, doi:10.1002/2014JC010212, 2014.

Vialard,. J. P. and co-authors.: Air-Sea Interactions in the Seychelles-Chagos Thermocline Ridge Region, BAMS, doi:10.1175/2008BAMS2499.1, 2009.

Vinayachandran P. N., Shankar D., S. Vernekar, K. K. Sandeep, P. Amol, C. P. Neema and A. Chatterjee.: A summer monsoon pump to keep the bay of Bengal salty, Geophys. Res. Lett., 40, 1777 – 1782, doi:10.1002/grl.50274, 2013.

Vinayachandran P. N., Yamagata, T.: Monsoon Response of the Sea around Sri Lanka: Generation of Thermal Domes and Anticyclonic Vortices, J. Phy. Oceano., 28, 1946 – 1960, doi: 10.1175/1520-0485, 1998.

Vinayachandran, P. N., Chauhan, P., Mohan, M., Nayak, S.: Biological response of the sea around Sri Lanka to summer monsoon, Geophys. Res. Lett., 31, L0I302, doi:10.1029/2003GL018533, 2004.

~~Vinayachandran, P. N., Mathew, S.: Phytoplankton bloom in the Bay of Bengal during the northeast monsoon and its intensification by cyclones, Geophy. Res. Lett., 30(11), 1572, doi:10.1029/2002GL016717, 2003.~~

Wang .X. J., Behrenfeld. M., Le Borgne .R., Murtugudde .R., and Boss. E.: Regulation of phytoplankton carbon to chlorophyll ratio by light, nutrients and temperature in the equatorial Pacific Ocean: a basin-scale model. Biogeosciences., 6, 391 – 404, doi:10.5194/bg-6-391-2009, 2009.

Wiggert J. D., Jones. B. H., Dickey .T D., Brink .K. H., Weller .R .A., Marra. J., Codispoti. L. A.: The Northeast Monsoon's impact on mixing, phytoplankton biomass and nutrient cycling in the Arabian Sea, Deep Sea Res. Pt. II, 47, 1353-1385, doi:10.1016/S0967-0645(99)00147-2, 2000.

Wiggert, J. D., Hood, R. R., Banse, K., Kindle, J. C.: Monsoon-driven biogeochemical processes in the Arabian Sea, Progr. Oceanogr., 65, 176-213, doi:10.1016/j.pocean.2005.03.008, 2005.

1046 Wiggert. J. D., Murtugudde, R. G., Christian J. R.: Annual ecosystem variability in the tropical
1047 Indian Ocean: results of a coupled bio-physical ocean general circulation model, Deep Sea Res.
1048 Pt. II., 53, 644-676, doi:10.1016/j.dsr2.2006.01.027, 2006.

1049 Xie, S. P., Annamalai, H., Schott, F. A., McCreary Jr. J. P.: Structure and mechanism of south
1050 Indian ocean climate variability, J. clim., 15, 864 – 878, doi: 10.1175/1520-0442, 2002.

1051 Xing W., Xiaomei. L., Haigang Z., Hailong. L.: Estimates of potential new production in the
1052 Java-Sumatra upwelling system, Chinese Journal of Oceanology and Limnology., 30, 1063-
1053 1067, doi:10.1007/s00343-012-1281, 2012.

1054 Yamanaka, Y., Yoshie, N, MasahikoFujii, Maka .N. Aita and Kishi. M. J.: An Ecosystem
1055 coupled with Nitrogen-Silicon-Carbon cycles applied to station A7 in the Northwestern Pacific,
1056 J. of Oceanogr., 60, p227-241, doi: 10.1023/B:JOCE.0000038329.91976.7d, 2004.

1057 Zhou X., Weng. E., Luo., Y.: Modelling patterns of nonlinearity in the ecosystem responses to
1058 temperature, CO_2 and precipitation changes, Eco. Appli., 18, 453 – 466, doi: 10.1890/07-0626.1,
1059 2008.

Table: 1 WAS = Western Arabian Sea, SLD = Sri Lanka Dome, SC = Sumatra Coast, SCTR = Seychelles-Chagos Thermocline Ridge. JJAS mean and ~~C~~climatological annual mean of CO_2 flux from Takahashi observations, constZc and varZc simulations. Units are ~~in~~ mol m^{-2} yr^{-1}.

Regions	CO_2 flux (mol m^{-2} yr^{-1})					
	JJAS Mean			Annual Mean		
	OBS	constZc	varZc	OBS	constZc	varZc
WAS	1.99	1.44 ± 0.2	2.31 ± 0.4	0.94	0.80 ± 0.1	1.07 ± 0.2
SLD	1.79	-0.008 ± 0.2	0.24 ± 0.09	0.80	-0.02 ± 0.1	0.10 ± 0.2
SC	0.31	0.60 ± 0.5	1.51 ± 1.01	0.21	0.21 ± 0.3	0.53 ± 0.5
SCTR	0.82	-0.32 ± 0.3	-0.05 ± 0.4	0.55	-0.02 ± 0.1	-0.07 ± 0.2

Table: 2 Same as Table 1, but for pCO_2. Units are ~~in~~ µatm.

Regions	pCO_2 (µatm)					
	JJAS Mean			Annual Mean		
	OBS	constZc	varZc	OBS	constZc	varZc
WAS	397.58	389.18 ± 3.7	399.95 ± 5.01	394.69	389.62 ± 3.9	391.19 ± 4.7
SLD	382.44	371.67 ± 6.04	379.24 ± 8.9	380.21	370.76 ± 6.1	374.94 ± 9.6
SC	372.52	382.36 ± 12.7	402.14 ± 21.8	372.69	374.65 ± 9.3	381.76 ± 13.6
SCTR	377.18	365.71 ± 5.08	370.72 ± 7.4	379.89	372.69 ± 4.7	369.00 ± 5.4

Table: 3 JJAS mean and ~~C~~climatological annual mean of Export production from satellite derived Net Primary Production data, constZc and varZc simulations. Units are ~~in~~ g C m^{-2} yr^{-1}.

Regions	Export Production (g C m^{-2} yr^{-1})					
	JJAS Mean			Annual Mean		
	OBS	constZc	varZc	OBS	constZc	varZc
WAS	123.57	84.81 ± 16.04	147.19 ± 23.8	94.31	77.41 ± 15.1	122.54 ± 25.2
SLD	51.54	167.71 ± 59.04	151.51 ± 46.4	43.25	144.43 ± 49.8	156.08 ± 43.8
SC	58.87	260.11 ± 104.7	310.03 ± 99.5	54.53	172.52 ± 72.4	215.52 ± 70.8
SCTR	51.08	57.39 ± 14.2	99.23 ± 21.8	40.45	55.15 ± 17.9	80.35 ± 26.04

Table: 4 Same as Table 3, but for New production.

Regions	New Production (g C m^{-2} yr^{-1})					
	JJAS Mean			Annual Mean		
	OBS	constZc	varZc	OBS	constZc	varZc
WAS	--	150.84 ± 27.9	133.03 ± 19.5	--	108.43 ± 23.4	81.47 ± 15.7
SLD	--	141.93 ± 64.1	77.78 ± 27.6	--	111.05 ± 71.1	50.37 ± 26.3
SC	--	63.64 ± 30.9	78.11 ± 29.1	--	56.69 ± 43.3	54.58 ± 23.3
SCTR	--	12.17 ± 16.3	13.32 ± 18.6	--	13.74 ± 15.5	12.94 ± 13

Table 5: Biological pump impact over DIC in the model due to constZc and varZc simulations for JJAS and Annual mean.

Biological Pump ($gC\ m^{-2}\ yr^{-1}$)	**constZc**		**varZc**	
	JJAS Mean	**Annual Mean**	**JJAS Mean**	**Annual Mean**
WAS	45.18 ± 14.8	45.49 ± 14.38	151.7 ± 23.8	126.67 ± 24.3
SLD	89.39 ± 58.1	108.65 ± 48.6	156.07 ± 48.4	161.15 ± 43.5
SC	235.54 ± 95.4	155.21 ± 67.4	319.16 ± 94.9	222.92 ± 68.7
SCTR	30.49 ± 13.4	26.81 ± 16.8	103.13 ± 19.6	83.98 ± 23.6

Table 6: Same as Table 5, But for Solubility pump.

Solubility Pump ($gC\ m^{-2}\ yr^{-1}$)	**constZc**		**varZc**	
	JJAS Mean	**Annual Mean**	**JJAS Mean**	**Annual Mean**
WAS	17.29 ± 3.5	9.63 ± 2.1	27.72 ± 4.8	12.92 ± 2.7
SLD	-0.09 ± 2.4	-0.32 ± 2.3	2.9 ± 3.5	1.31 ± 3.5
SC	7.22 ± 6.9	2.56 ± 3.8	18.17 ± 12.1	6.43 ± 6.0
SCTR	-3.95 ± 3.7	-0.35 ± 2.3	-0.61 ± 5.3	-0.86 ± 2.8

Table ~~5~~7: Table shows JJAS mean and climatological annual mean response from the model forced with annual mean currents.

WAS region forced with Annual mean currents	JJAS mean		Improvement	Climatological Annual mean		Improvement
CO_2 flux (mol m^{-2} yr^{-1})	0.80 ± 0.2	1.29 ± 0.2	0.48 ± 0.04	0.65 ± 0.1	0.79 ± 0.1	0.13 ± 0.02
pCO_2 (µatm)	381.81 ± 3.4	387.24 ± 3.9	5.43 ± 0.5	388.68 ± 3.4	388.40 ± 3.6	-0.28 ± 0.1
Export production (g C m^{-2} yr^{-1})	60.71 ± 4.7	104.22 ± 13.4	43.51 ± 8.6	74.30 ± 4.5	104.58 ± 18.3	30.28 ± 13.7
New Production (g C m^{-2} yr^{-1})	34.76 ± 2.3	52.16 ± 1.51	17.39 ± 0.8	29.91 ± 1.7	44.72 ± 1.6	14.81 ± 0.1

Table ~~6~~8 Same as Table ~~5~~7 but from annual mean temperature simulations.

WAS region forced with Annual mean temperature	JJAS mean		Improvement	Climatological Annual mean		Improvement
	constZc	varZc		constZc	varZc	
CO_2 flux (mol m^{-2} yr^{-1})	1.85 ± 0.2	2.74 ± 0.4	0.88 ± 0.1	0.81 ± 0.1	1.10 ± 0.2	0.28 ± 0.07
pCO_2 (µatm)	393.20 ± 3.01	404.26 ± 4.9	11.05 ± 1.9	384.61 ± 3.3	386.52 ± 4.8	1.91 ± 1.4

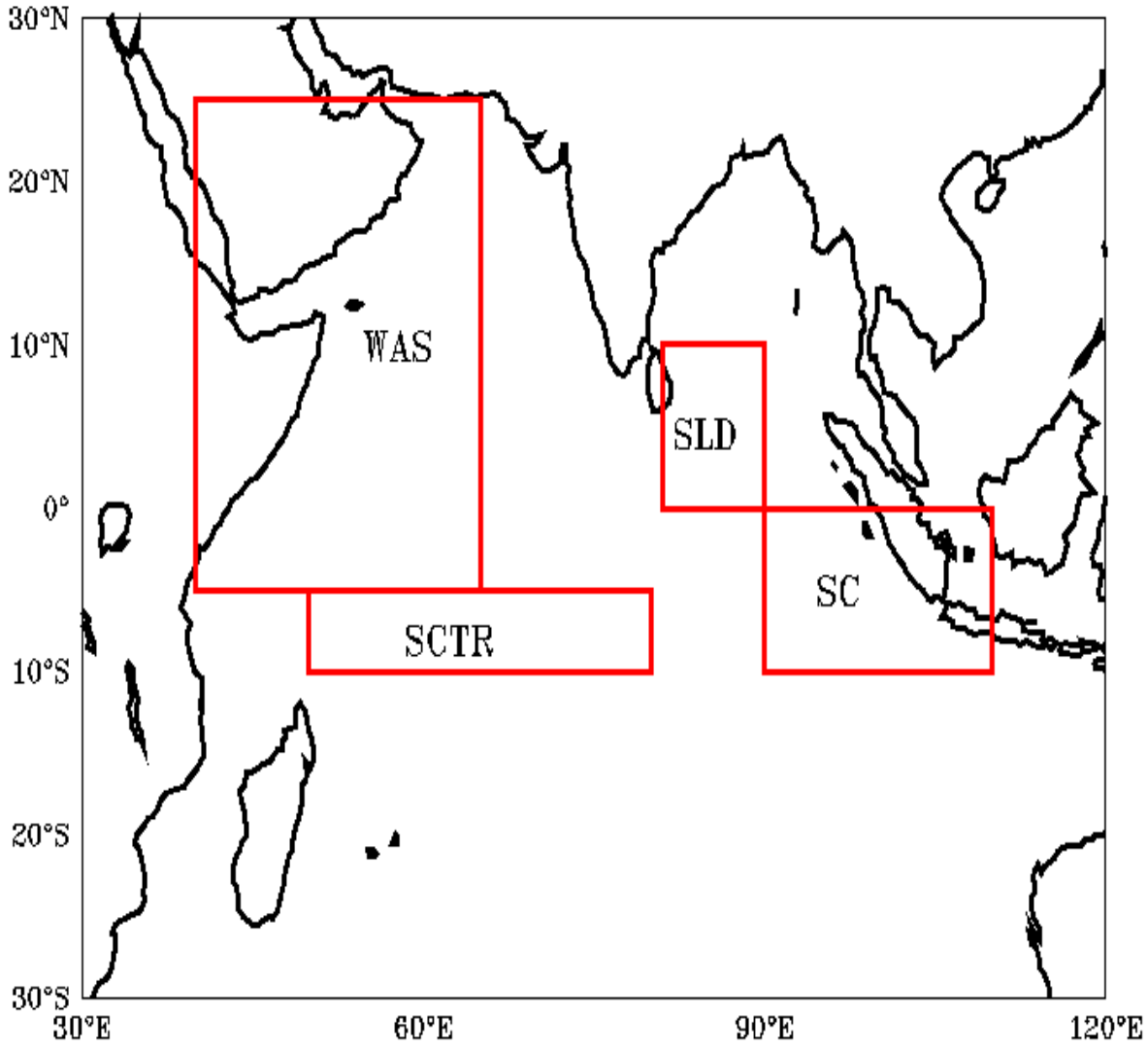

Figure 1 Red boxes shows the study regions (1) WAS (Western Arabian Sea: ~~[~~40°E:65°E, 5°S:25°N~~]~~) (2) SLD (Srilanka~~n~~ Dome: ~~[~~81°E:90°E, 0°:10°N~~]~~) (3) SCTR (Seychelles-Chagos Thermocline Ridge: ~~[~~50°E:80°E, 5°S:10°S~~]~~) and (4) SC (Sumatra Coast: ~~[~~90°E:110°E, 0°:10°S~~]~~).

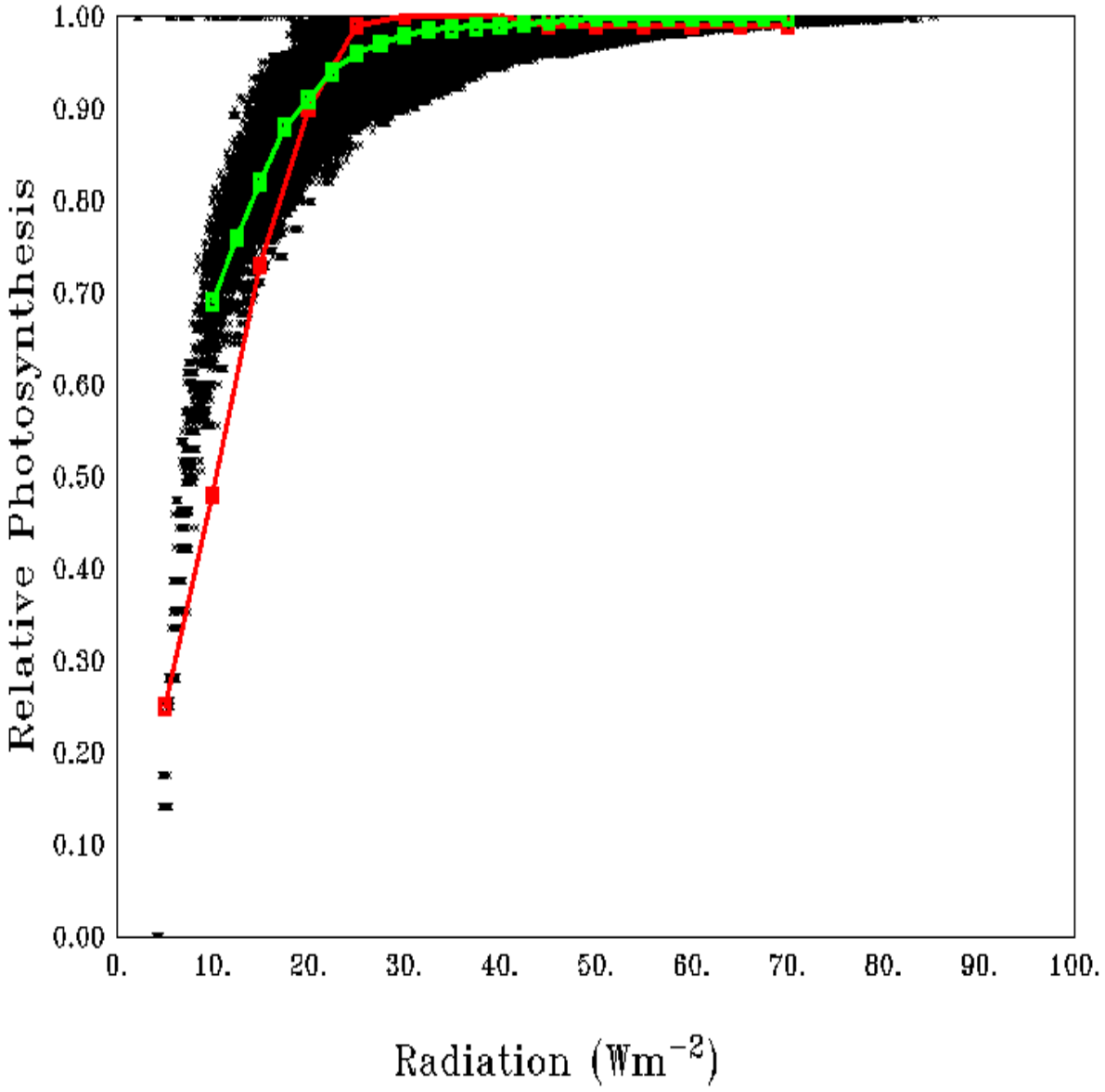

Figure ~~(2)~~: ~~P – I curve,~~ Scatter of~~or~~ average relative photosynthesis ~~against~~versus different light intensities in the model (black dots) and its mean (green curve). Red curve shows the theoretical P – I curve from Parsons et al., (1984). ~~Green curve shows average of the scatter in the model.~~

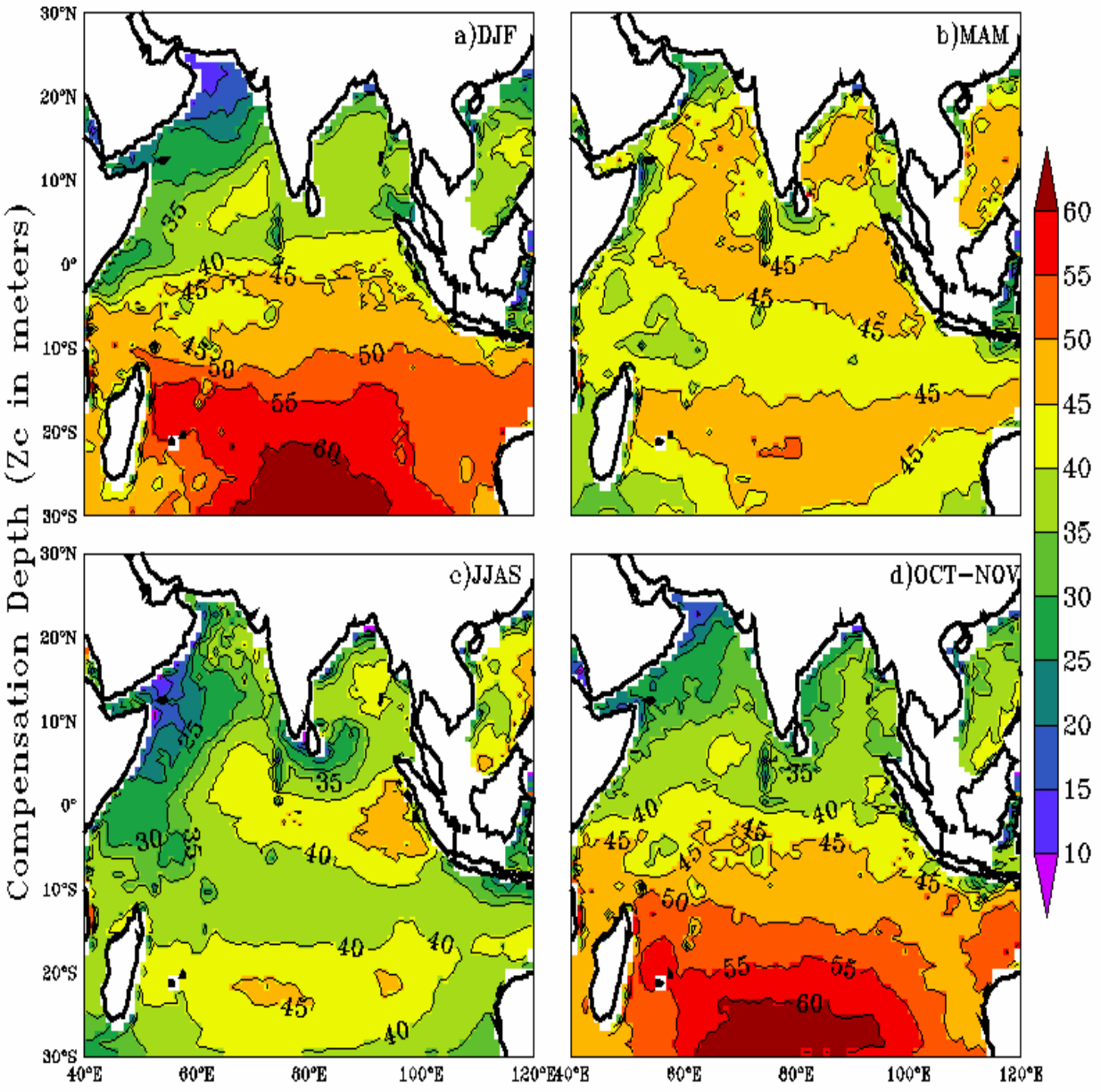

Figure ~~(~~3~~)~~: Seasonal mean maps of varying Compensation Depth (varZc) as a function of Chl-a and light (a) December to January (DJF), (b) March to May (MAM), (c) June to September (JJAS), (d) October to November (OCT-NOV). Units are ~~in~~ meters.

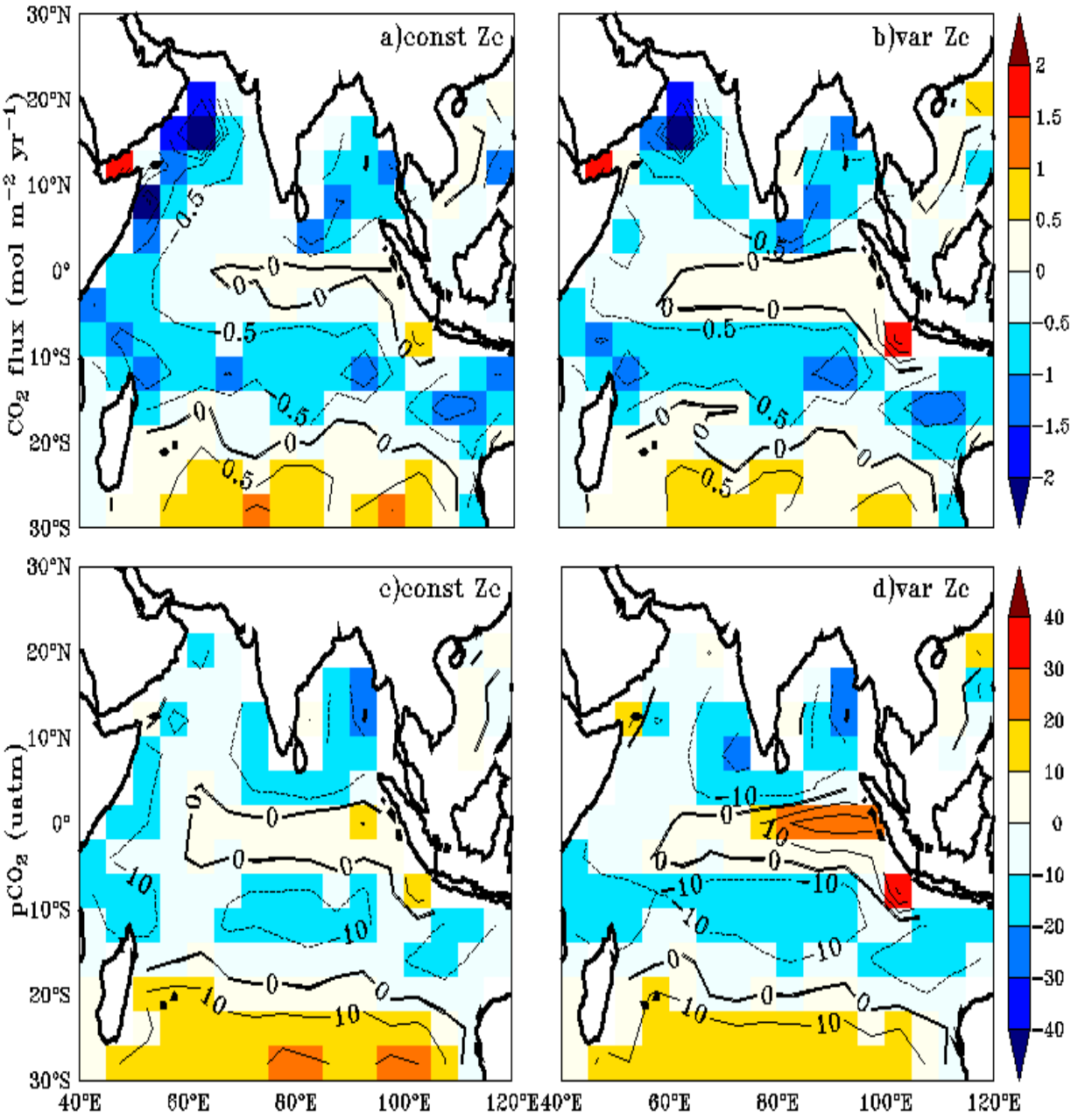

Figure ~~(4)~~: Annual mean biases in model evaluated against Takahashi et al., (2009) observations for CO_2 flux (a, b) and pCO_2 (c, d) with constant Zc (constZc) and Varying Zc (varZc). Units of CO_2 flux and pCO_2 are mol m^{-2} yr^{-1} and µatm respectively.

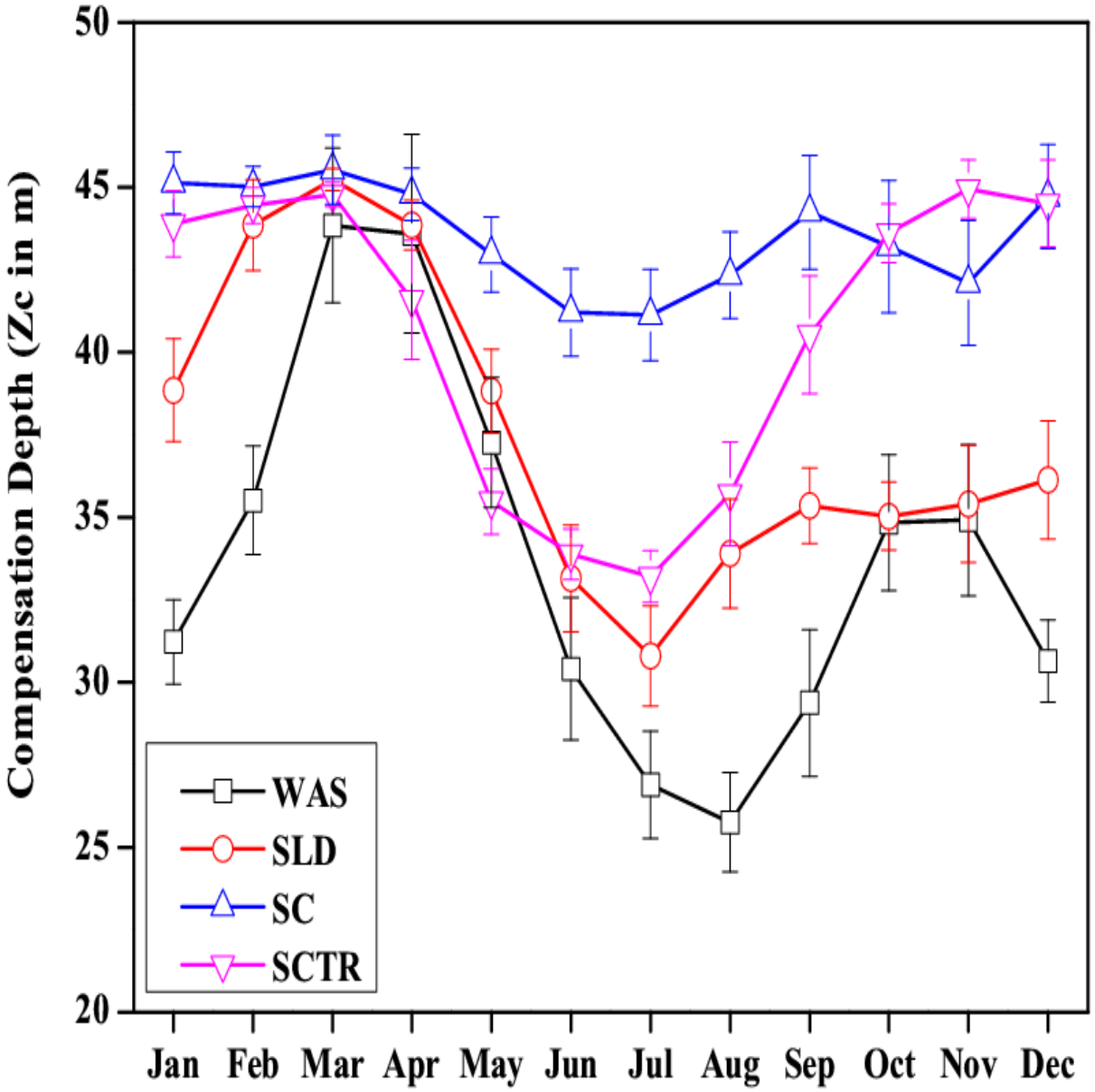

Figure ~~(5)~~: Seasonal variations in ~~compensation depth (~~varZc~~)~~ over the study regions shown as climatology~~ical state~~ computed over 1990-2010. Error bar shows standard deviations of individual months over these years. Units are ~~in~~ meters.

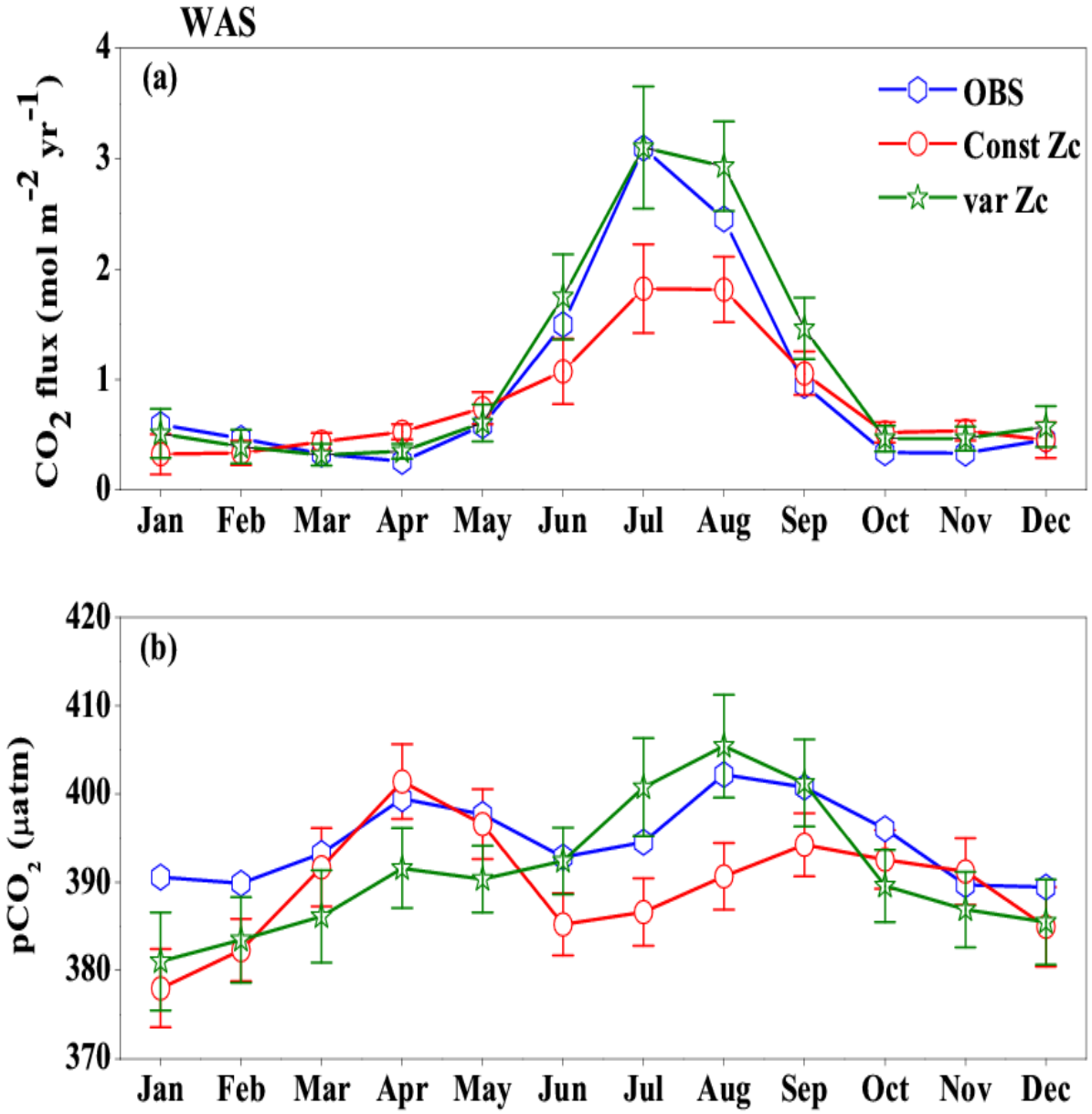

Figure ~~(~~6~~)~~: Comparison of model (a) CO_2 flux and (b) pCO_2 simulated with constant Zc (const Zc) and varying Zc (var Zc) with that of Takahashi et al., (2009) Observations (OBS) over Western Arabian Sea (WAS) region as climatological state computed over 1990-2010. Error bar shows standard deviations of individual months over these years. Units of CO_2 flux and pCO_2 are mol m^{-2} yr^{-1} and µatm respectively. Legend is common for both graphs.

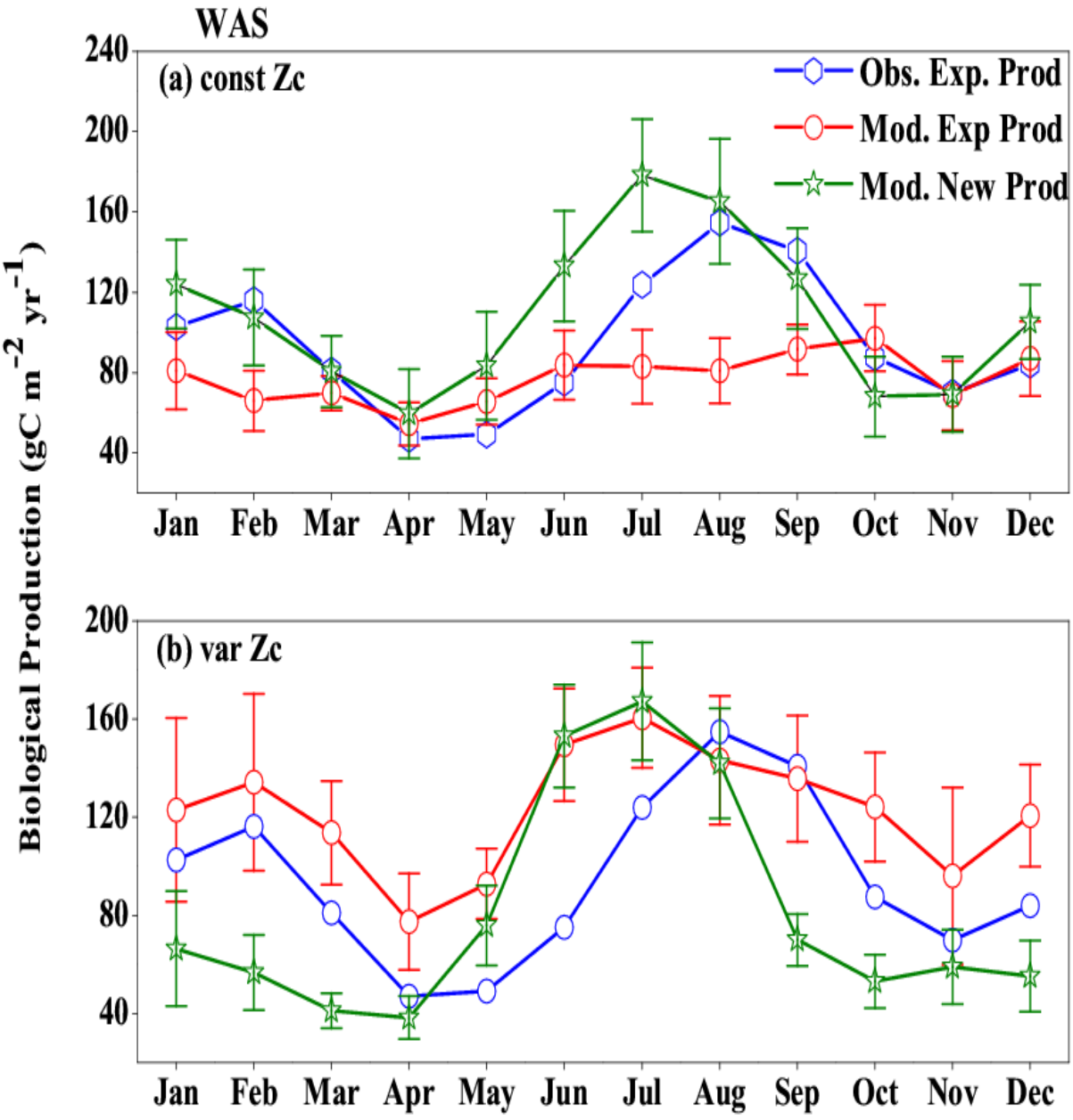

Figure ~~(~~7~~)~~: Comparison of model export production (Mod. Exp. Prod) and n~~N~~ew production (Mod. New Prod) with satellite derived export production (Obs. Exp. Prod) for (a) Const Zc and (b) var Zc simulations for Western Arabian Sea (WAS) region. Units are in g C m^{-2} yr^{-1}. Legends are common for both graphs.

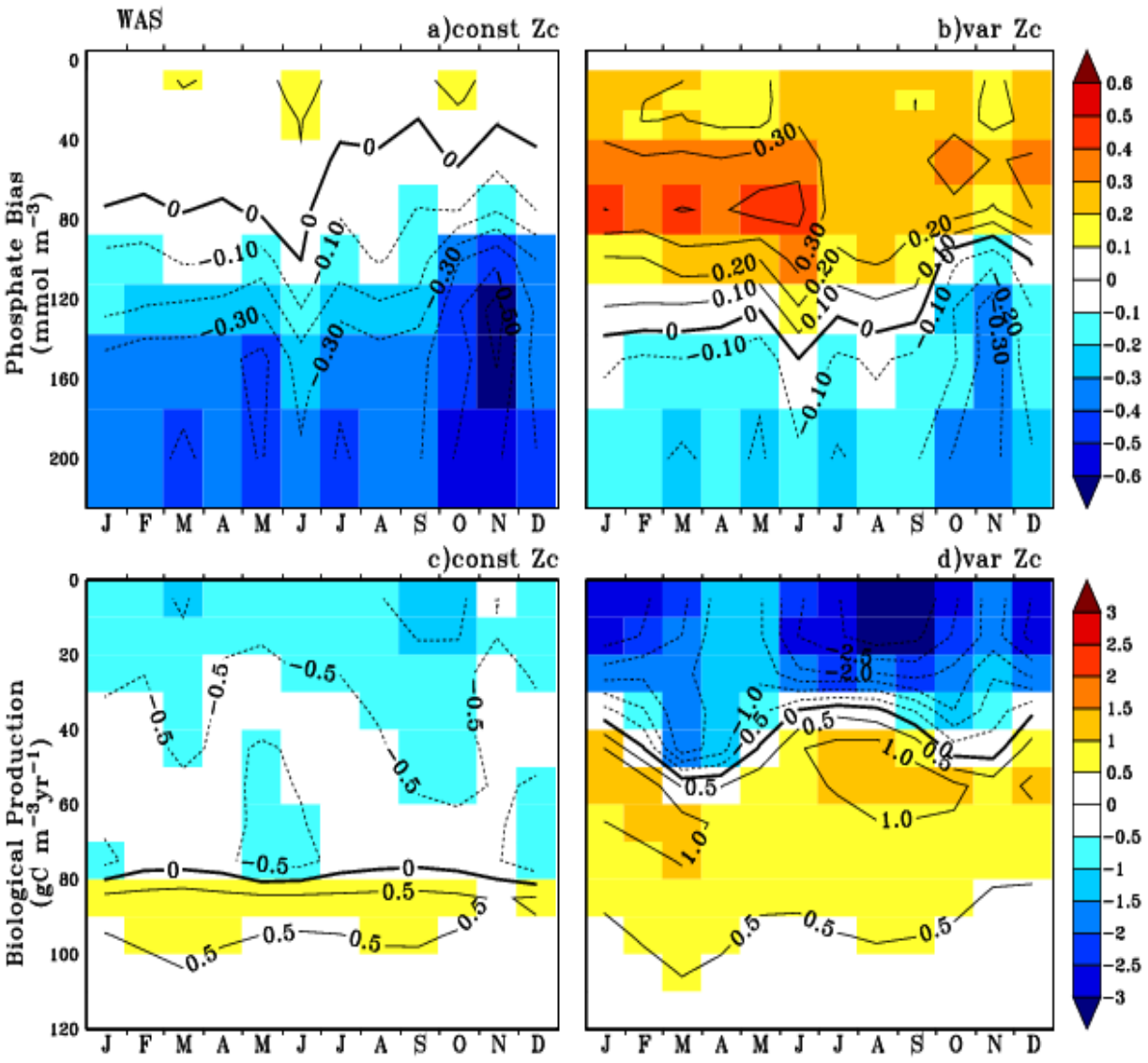

Figure 8: Annual mean bias of model phosphate when compared with climatological observational data (a) for constZc and (b) for varZc simulations. Corresponding annual mean biological source/sink profiles (c, d) in the model for WAS. Unit of phosphate is mmol m^{-3} and biological production is g C m^{-3} yr^{-1}.

~~Fig (8): Bias estimation of Phosphate in the model with climatological observational data (a) const Zc and (b) Var Zc simulations and corresponding Biological production (c, d) in the model for Western Arabian Sea (WAS) region. Units of Phosphate (x 100 mol m^{-3}) and Biological Production (g C m^{-3} yr^{-1}).~~

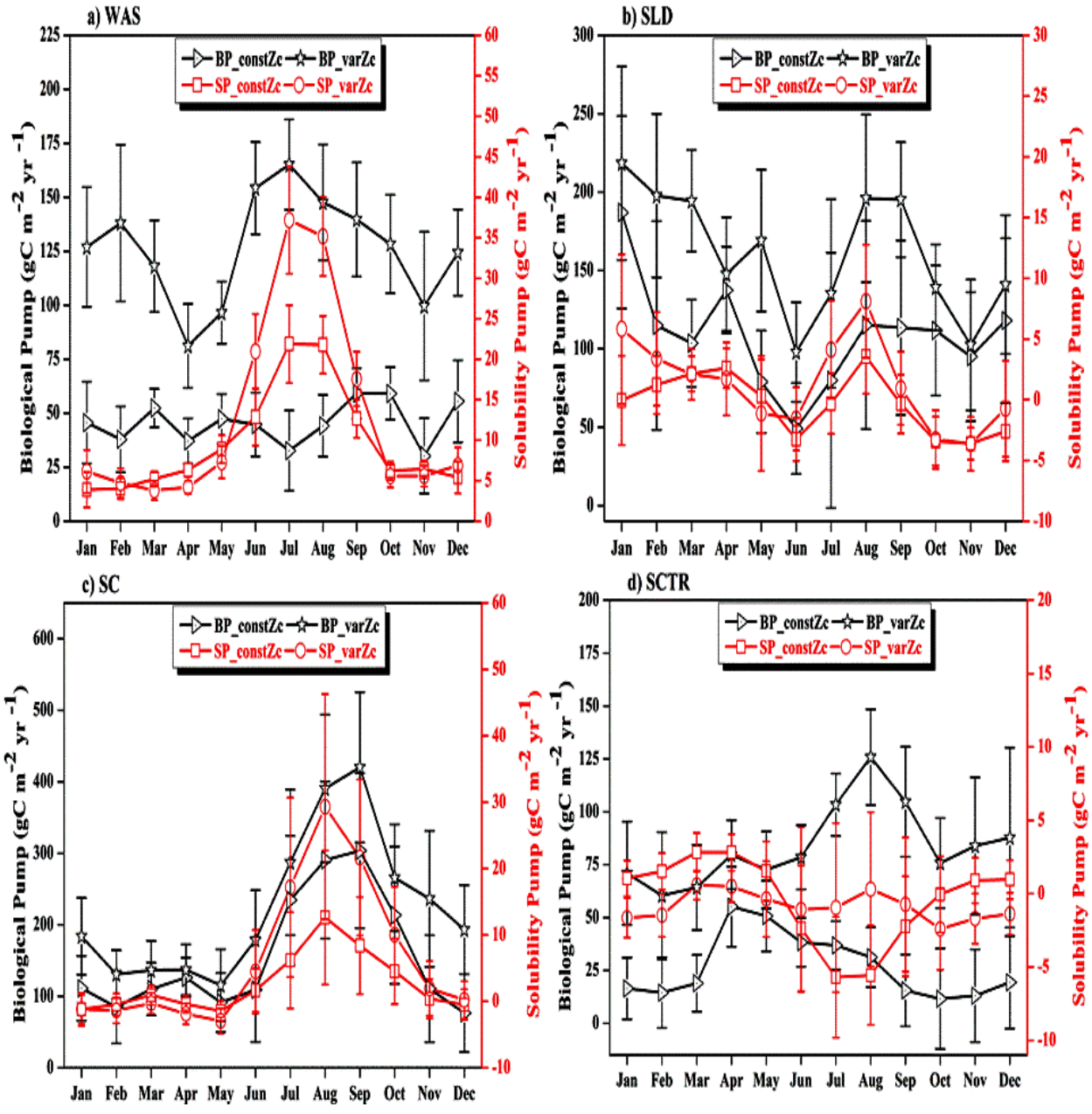

Figure 9: The strength of the biological pump (BP, black lines) and solubility pump (SP, red lines) from constZc and varZc simulations for (a) WAS (b) SLD (c) SC and (d) SCTR. The left axis shows the biological pump and the right axis shows the solubility pump. Error bar shows standard deviations of individual months over the years 1990 - 2010. Units are g C m^{-2} yr^{-1}.

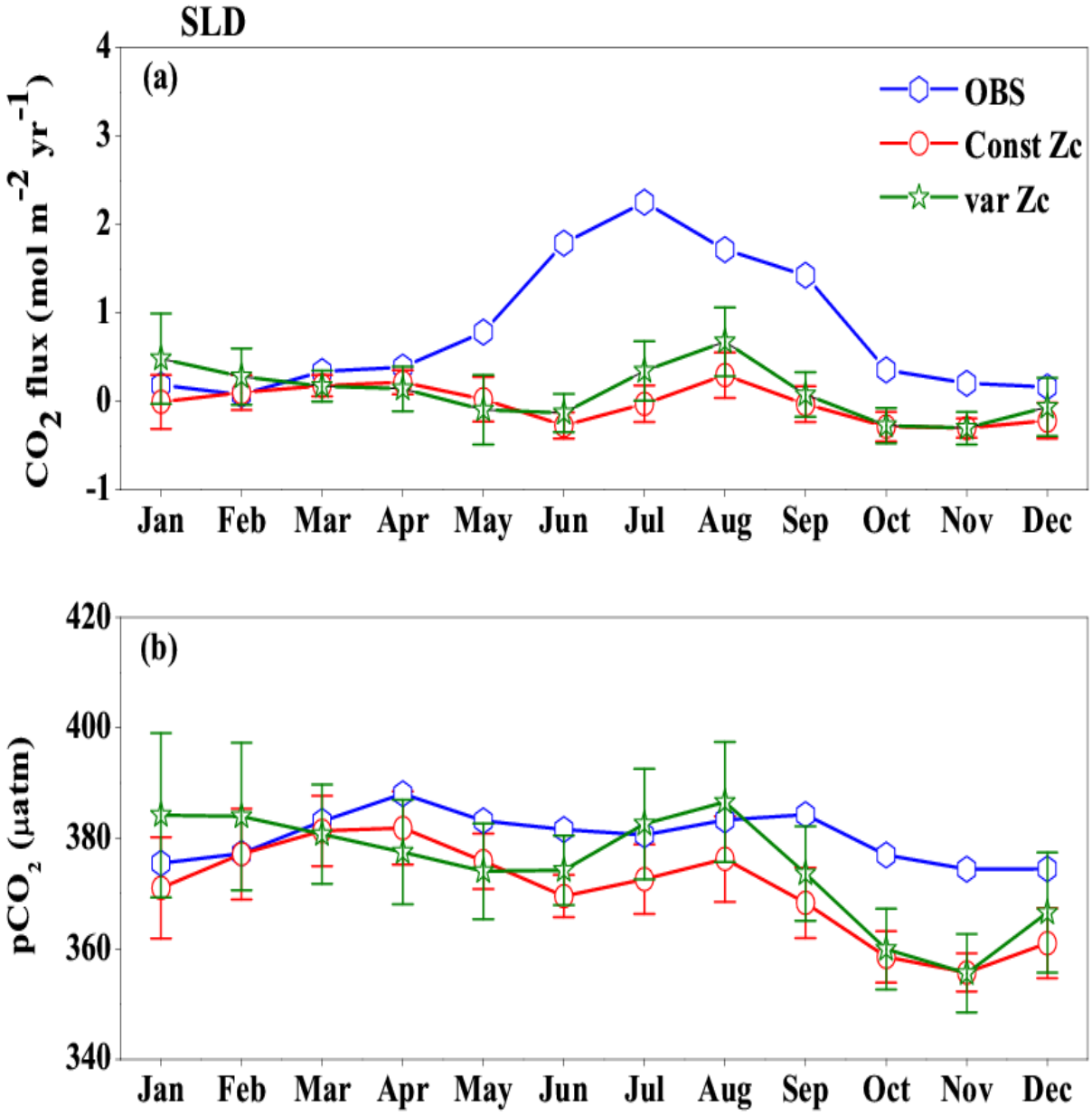

Figure 10: Same as Figure (6), but for SLD.

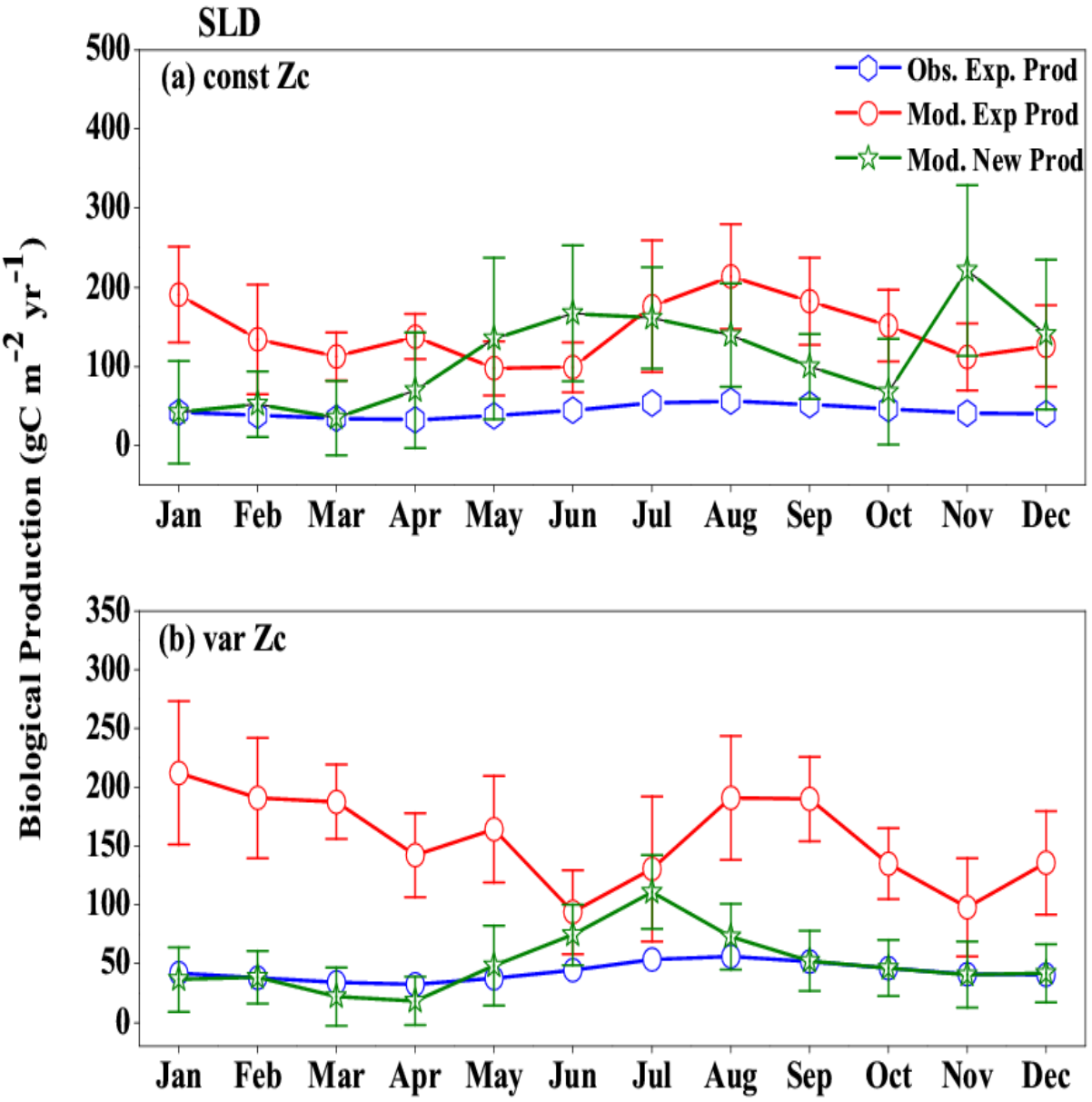

Figure 11: Same as Figure (7), but for SLD.

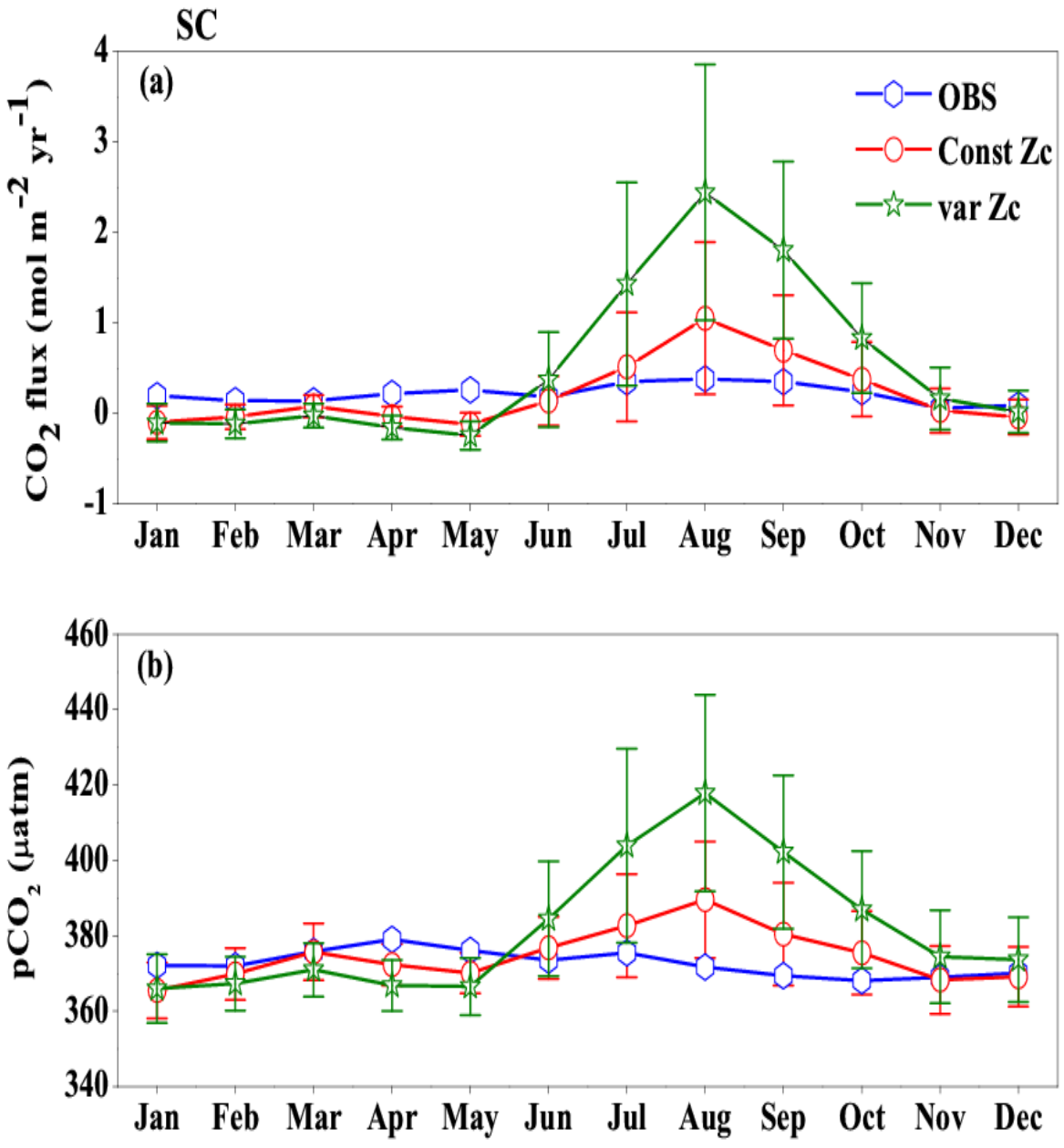

Figure 12: Same as Figure (6), but for SC.

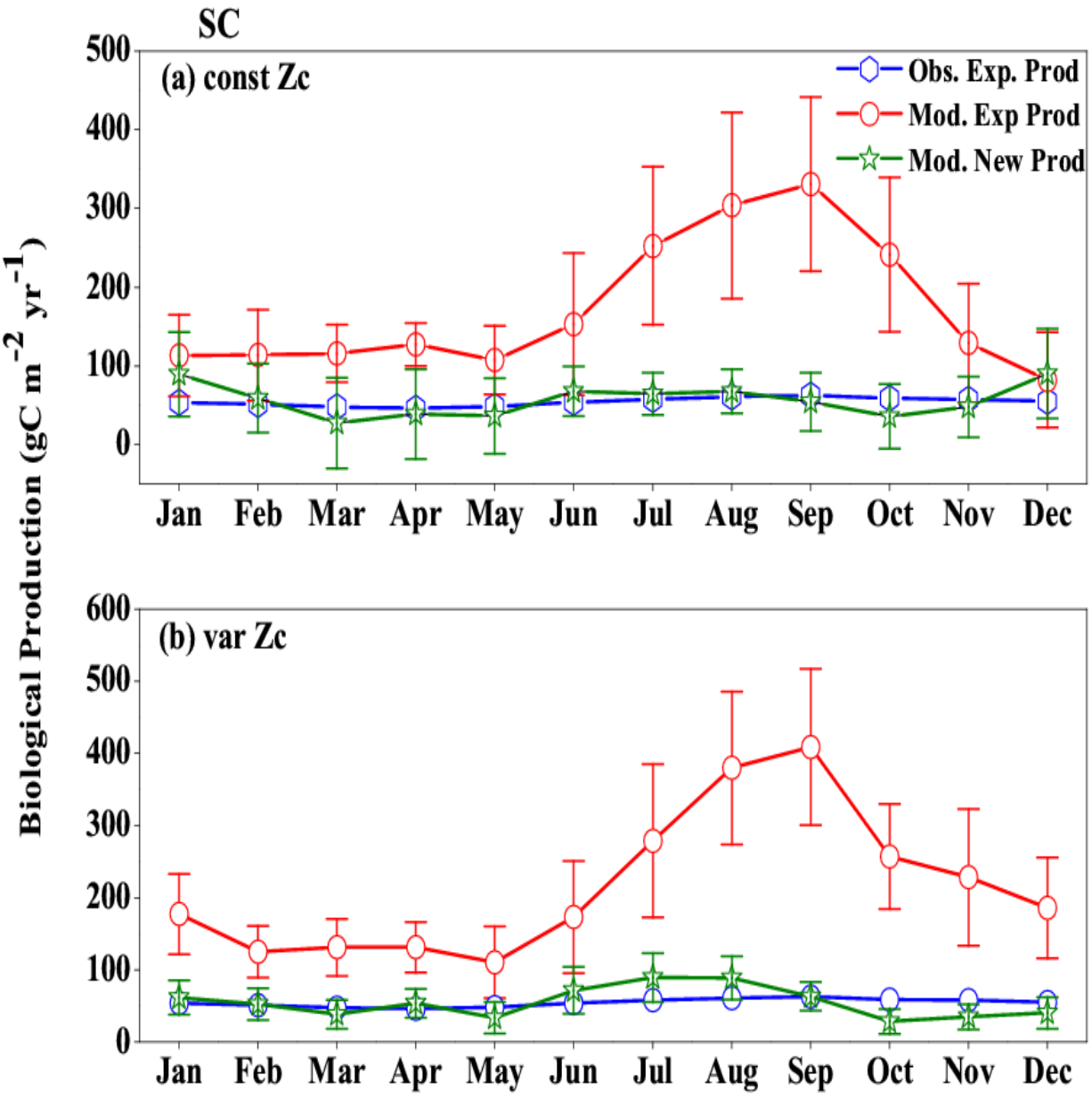

Figure 13: Same as Figure (7), but for SC.

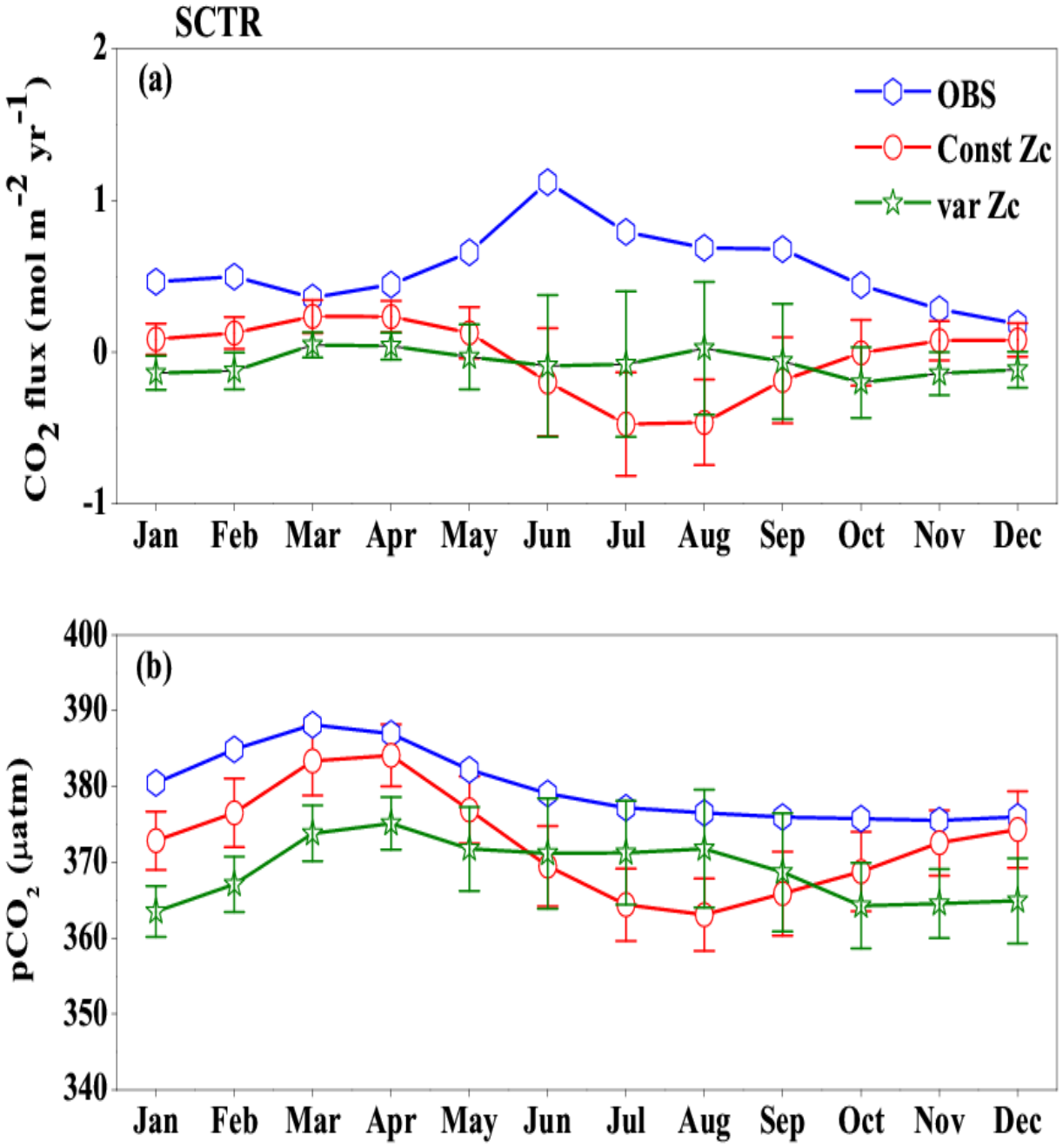

Figure 14: Same as Figure (6), but for SCTR.

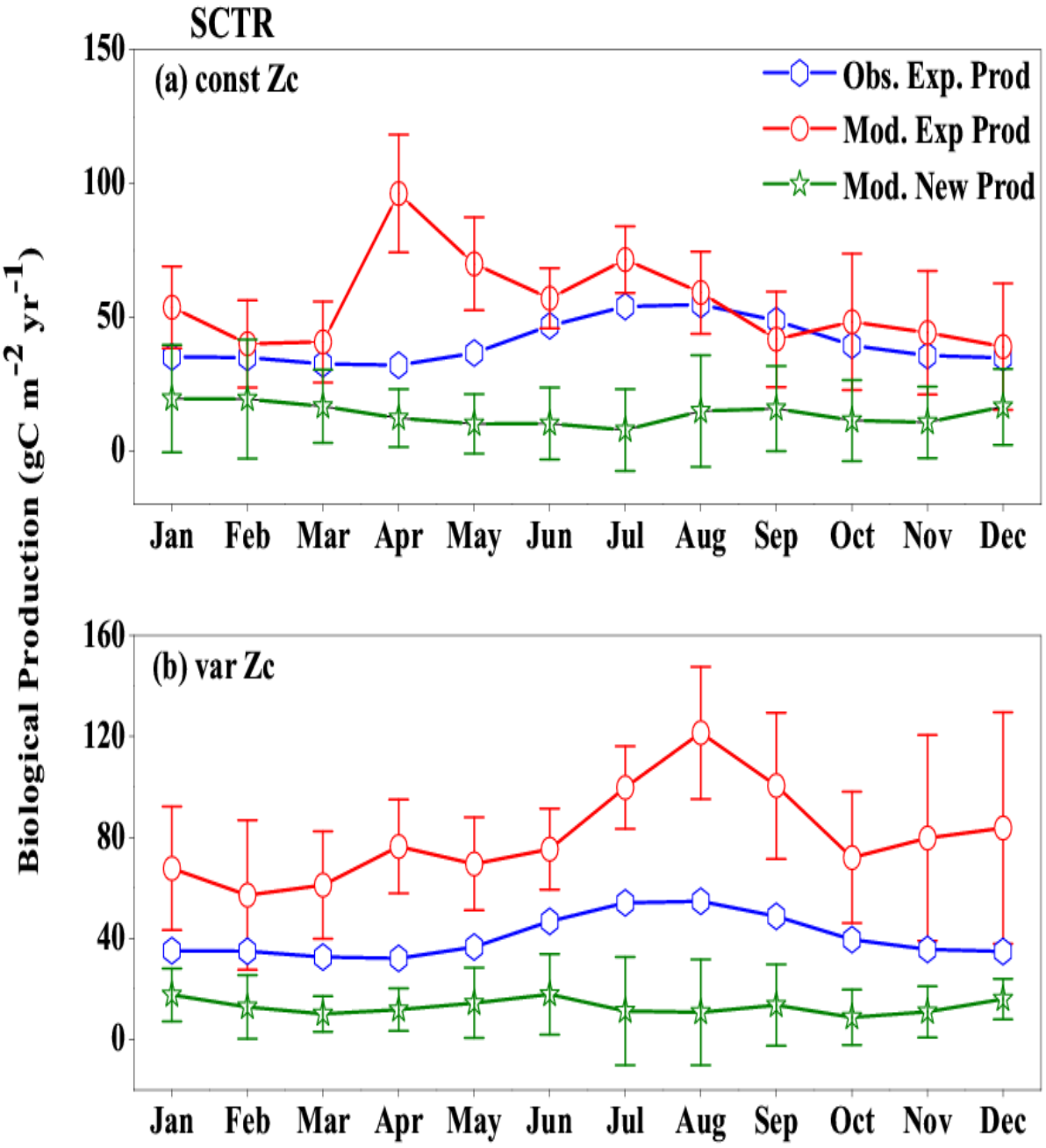

Figure 15: Same as Figure (7), but for SCTR.

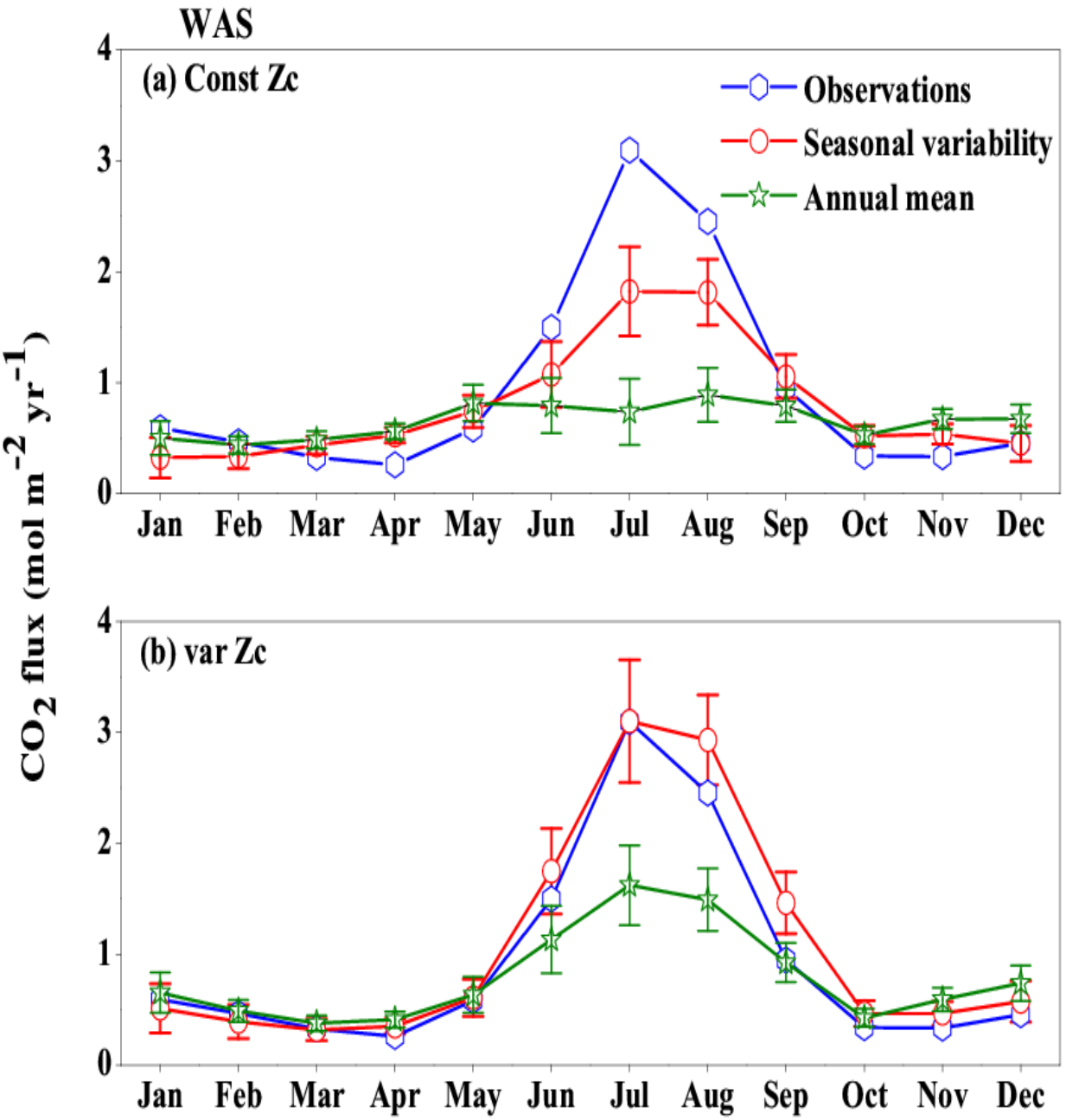

Figure 16: Response of CO_2 flux from the model forced with annual mean currents over the WAS as climatology computed over 1990-2010. Error bar shows standard deviations of individual months over these years. (a) constZc and (b) varZc. Units are mol m^{-2} yr^{-1}. Legends are same for both graphs.

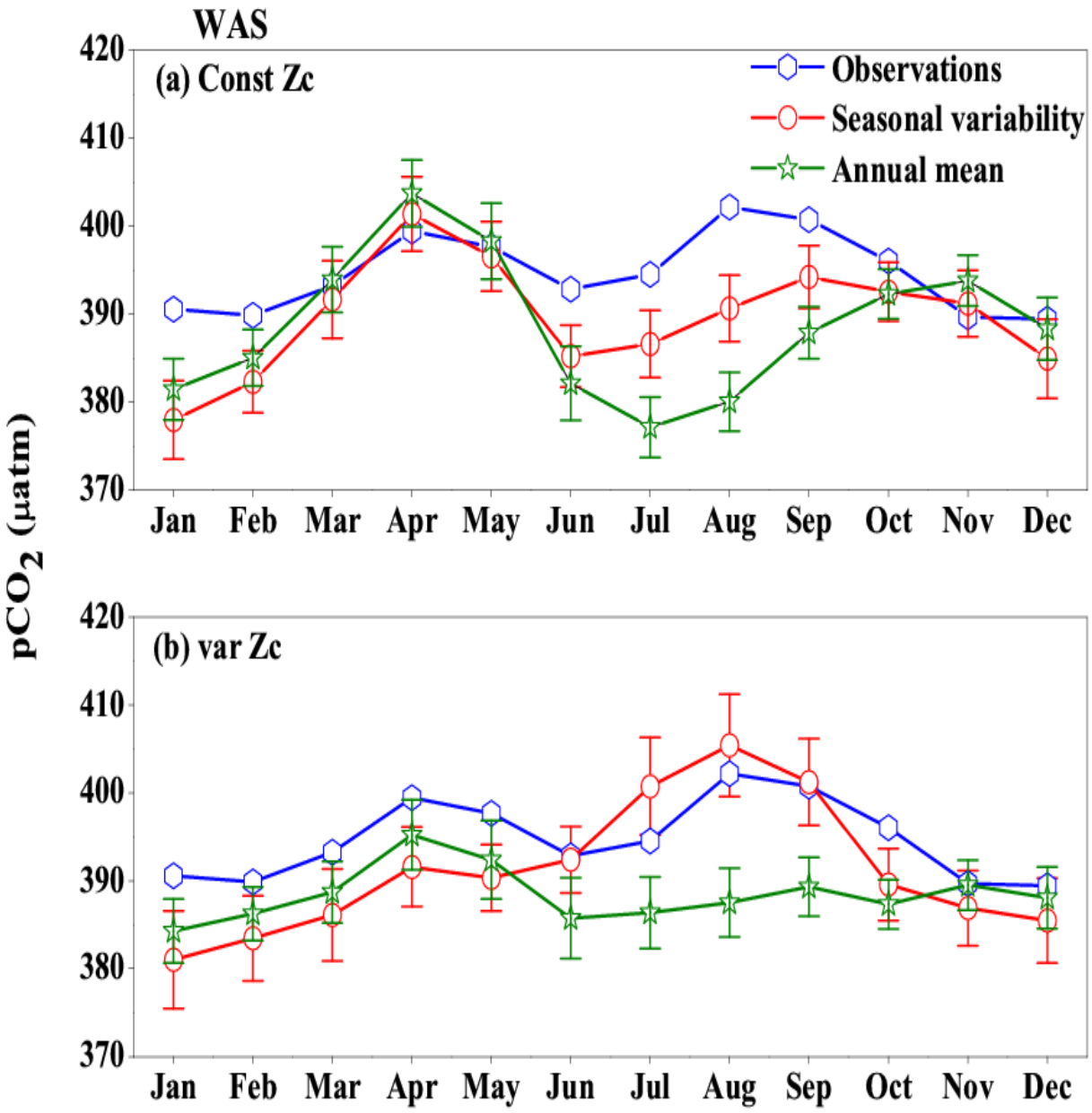

Figure 17: Same as Figure (16), but for pCO_2. Units are µatm.

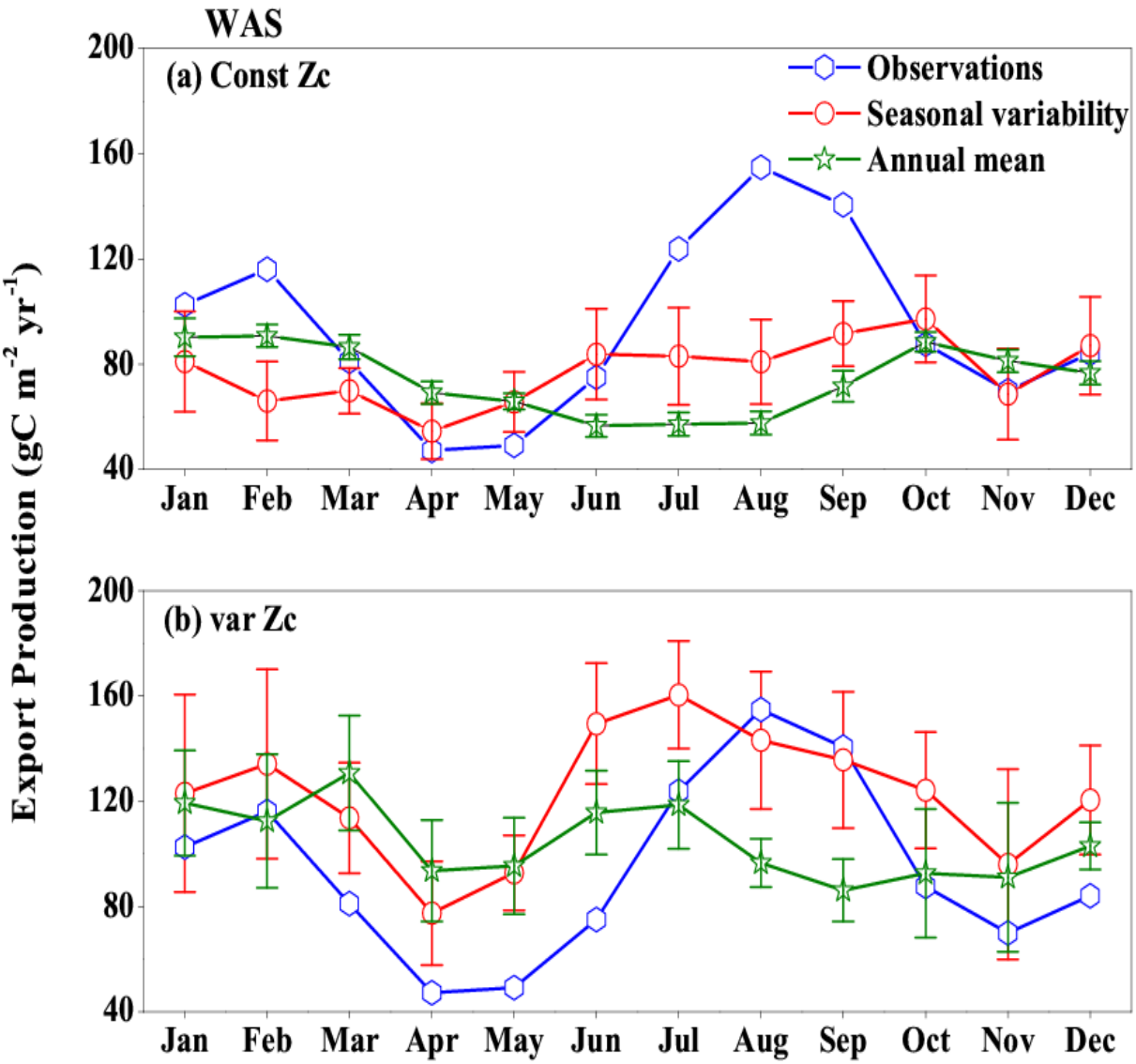

Figure 18: Response in export production of the model forced with annual mean currents in the WAS as climatology computed over 1990-2010. Error bar shows standard deviations of individual months over these years. (a) constZc (b) varZc. Units are g C m^{-2} yr^{-1}. Legends are same for both graphs.

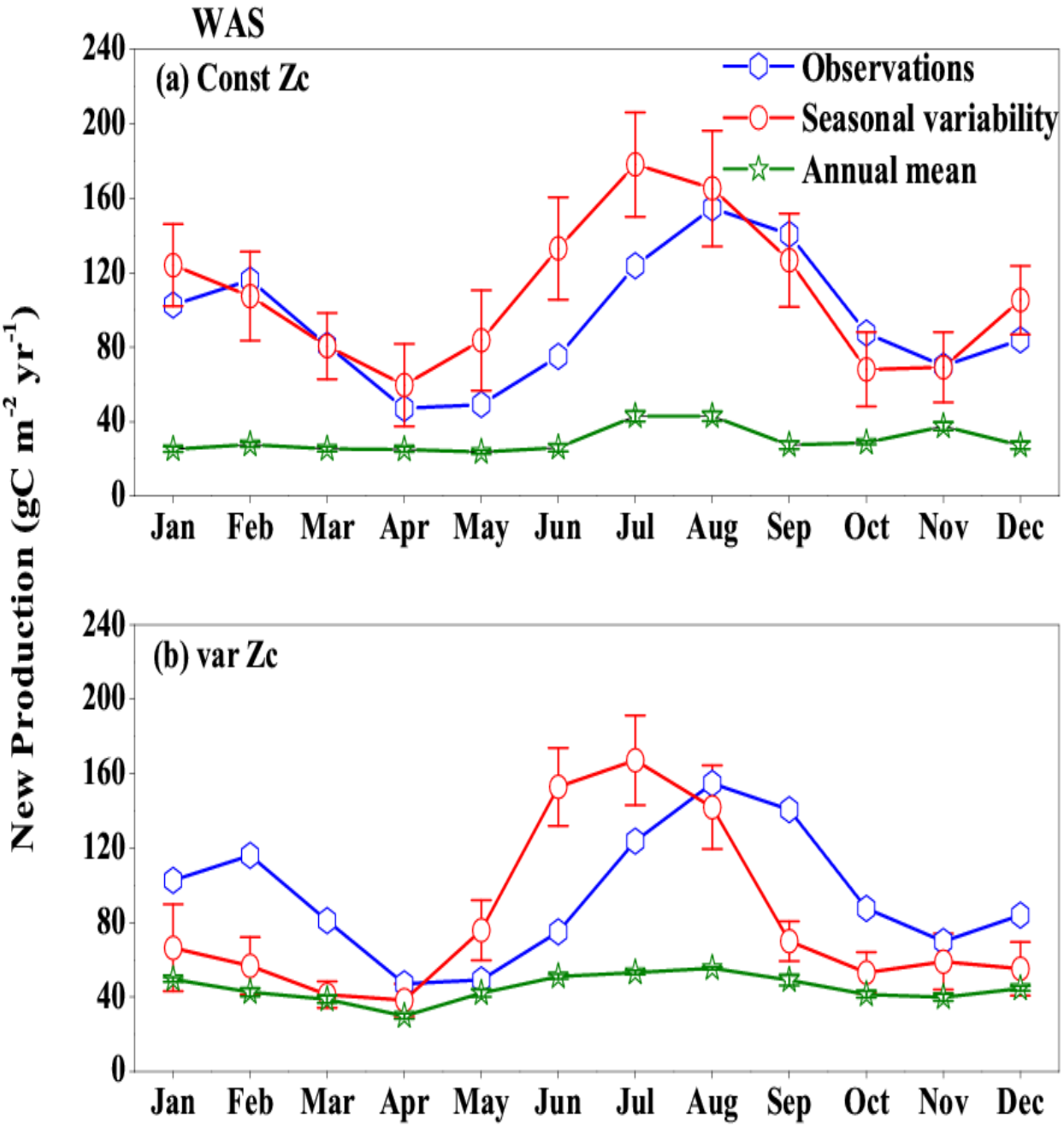

Figure 19: Same as Figure (18), but for New Production. Units are g C m^{-2} yr^{-1}.

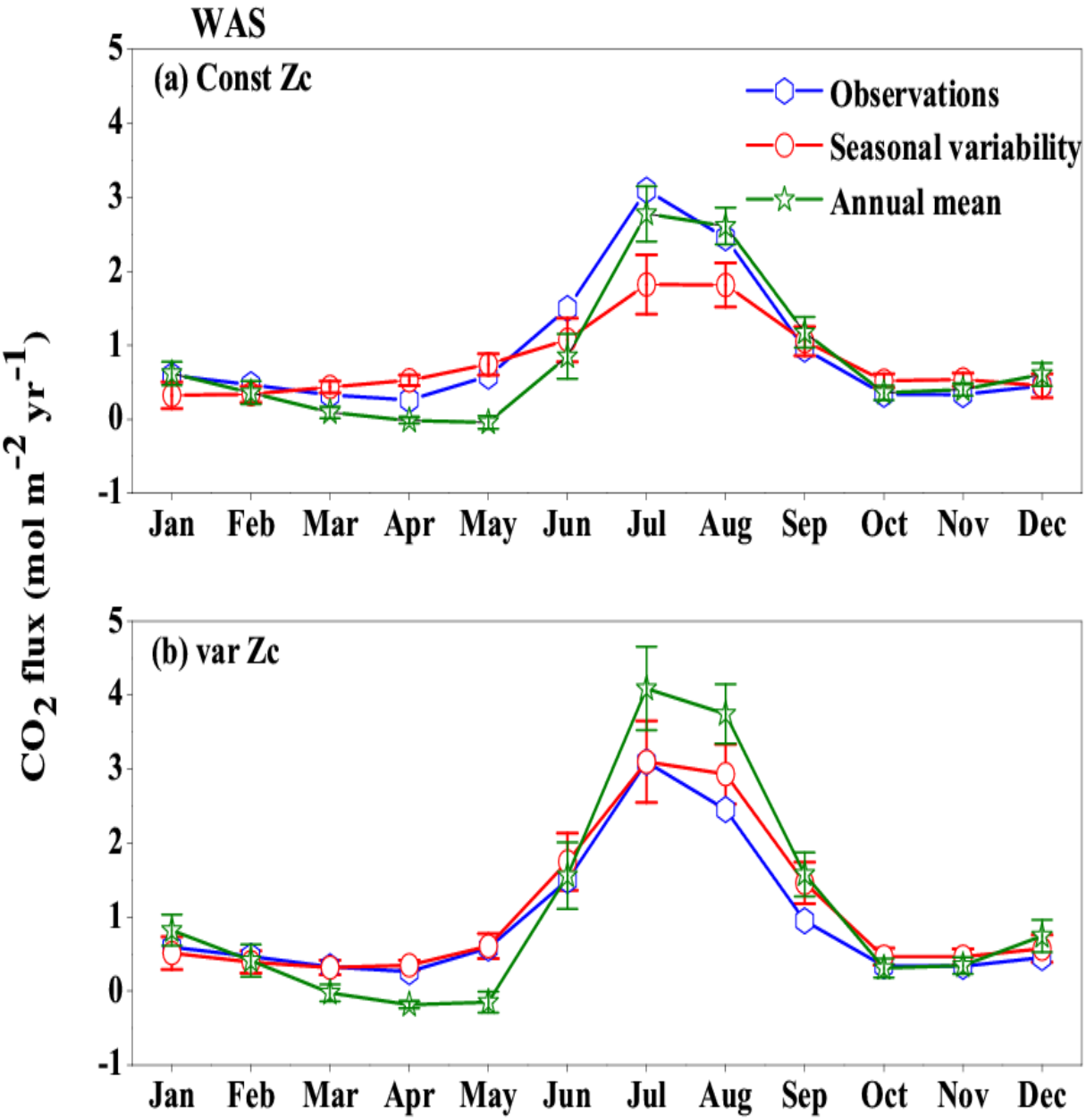

Figure 20: Response of CO_2 flux from the model forced with annual mean SST over the WAS as climatology computed over 1990-2010. Error bar shows standard deviations of individual months over these years. (a) constZc and (b) varZc. Units are mol m^{-2} yr^{-1}. Legends are same for both graphs.

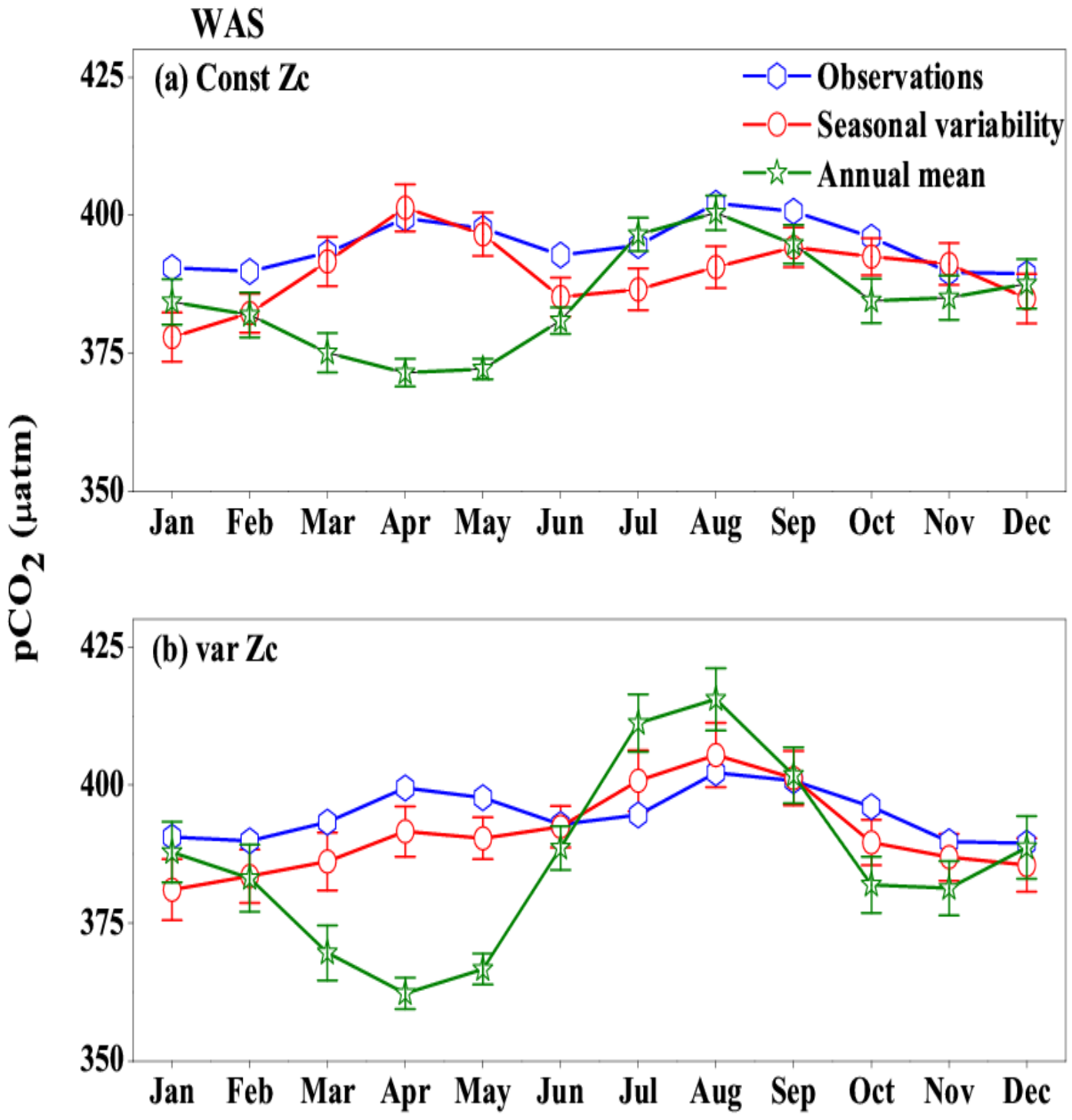

Figure 21: Same as Figure (20), But for pCO_2. Units are µatm.